JAERI-M
85-112

PROGRESS REPORT ON JAERI - ORNL COOPERATIVE NEUTRON SCATTERING RESEARCH APRIL 1, 1984 – MARCH 31, 1985

August 1985

Editor: Masashi IIZUMI

日本原子力研究所
Japan Atomic Energy Research Institute

JAERI-Mレポートは，日本原子力研究所が不定期に公刊している研究報告書です。

入手の問合わせは，日本原子力研究所技術情報部情報資料課（〒319－11茨城県那珂郡東海村）あて，お申しこしください。なお，このほかに財団法人原子力弘済会資料センター（〒319-11茨城県那珂郡東海村日本原子力研究所内）で複写による実費頒布をおこなっております。

JAERI-M reports are issued irregularly.

Inquiries about availability of the reports should be addressed to Information Division, Department of Technical Information, Japan Atomic Energy Research Institute, Tokai-mura, Naka-gun, Ibaraki-ken 319-11, Japan.

© Japan Atomic Energy Research Institute, 1985

編集兼発行　日本原子力研究所
印　　刷　日立高速印刷株式会社

JAERI-M 85-112

Progress Report on JAERI-ORNL Cooperative Neutron Scattering Research, April 1, 1984 -March 31, 1985

(Ed.) Masashi IIZUMI

Department of Physics
Tokai Research Establishment, JAERI

(Received July 6, 1985)

One year activities done under the JAERI-DOE(ORNL) cooperative neutron scattering program are summarized. This period just followed the completion of the wide-angle neutron diffractometer dedicated to the cooperative research. The report contains results of the performance test of the instrument and early research activities. The latter part includes the time-resolved measurements of the transition kinetics in tin and Ni-Mn alloy as well as the single-crystal diffraction by the flat-cone method.

Keywords: Neutron Diffraction, Neutron Scattering, Diffractometer, Phase Transition, Transition Kinetics, Time-resolved Measurement, Order-disorder Transition, Flat-cone method, Tin, Nickel-manganese Alloy

JAERI－M 85－112

原研－オークリッジ国立研中性子散乱協力研究プログレス・レポート
（1984年4月1日～1985年3月31日）

日本原子力研究所東海研究所物理部
（編）飯泉　仁

（1985年7月6日受理）

中性子散乱日米協力により，オークリッジ国立研でなされた研究活動を一年分まとめたものである。協力研究の主装置の広角中性子回折装置が完成した直後であるので，その性能テストの結果及び初期の研究結果が主な内容である。スズ及びNi－Mn合金における相転移カイネティクス，フラフトコーン法による単結晶回折法などの結果がのべられている。

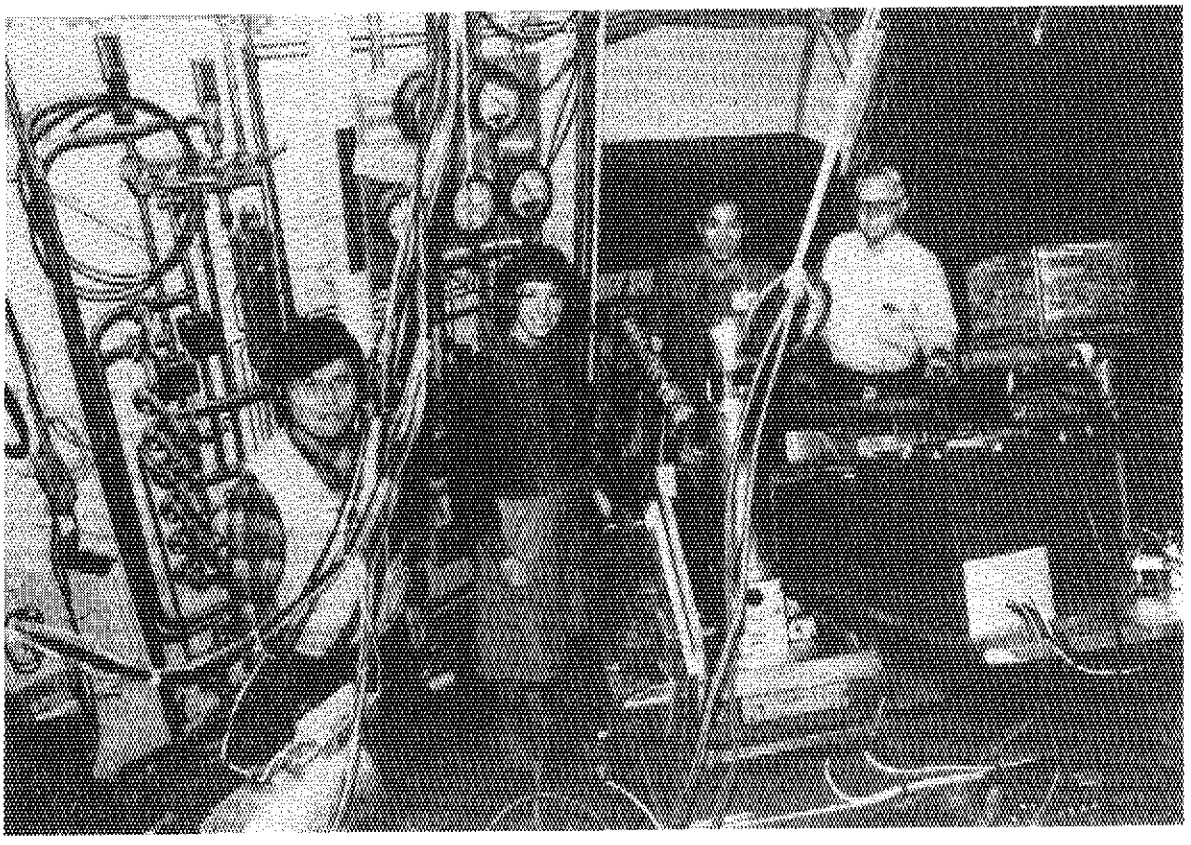

Wide-angle neutron diffractometer at the HB-4A beam hole of HFIR pictured together with the most active participants in the JAERI-ORNL program in FY-1984. They are from left to right Susumu Katano, Sharron King, Satoru Funahashi and Ray Child. Notice that the wide-angle neutron diffractometer is in an inclined position. The tube between Sharron and Satoru is the evacuated beam tube. A Displex cryostat system is on the crystal table.

CONTENTS

I. PREFACE

One year has passed since a rather strange instrument was installed in a corner of the crowded experimental floor of the HFIR (High Flux Isotope Reactor) of Oak Ridge National Laboratory. At a glance it is just a large lump of black blocks sitting on a track assembly. The instrument looks stranger when the upper body of the machine is inclined on the track assembly. One would have never seen the neutron scattering facility of that looks. This is the instrument dedicated to the JAERI-ORNL part of the US-Japan cooperative research in the field of neutron scattering. The instrument has given us a lot of excitement as well as a little headache for the past one year. In the present first issue of the progress report of the JAERI-ORNL Cooperative Research on Neutron Scattering we would like to record those activities taking place in the 1984 Japanese fiscal year (April 1, 1984 to March 31, 1985).

This past fiscal year was filled with significant achievement, as is shown in the following report. After several years of instrument designing and constructing and of discussions about research plans, it was particularly gratifying this year finally to be able to carry out experiments on the Wide-Angle Neutron Diffractometer. Beginning in April, evaluation and testing experiments were begun. The results of these experiments were both encouraging and a little discouraging. The data acquisition system, particularly the time-slicing features, the data display and analysis software, and the control of the diffractometer movements worked very well. However, certain aspects of the detector performance fell below our expectations, as discussed below. While we have hopes for improvements, nevertheless, several important experiments were carried out on the existing system. The great value of this diffractometer as a research tool for studying the kinetics of phase transitions and for studying both the Bragg reflections and the diffuse scattering in single crystals has been demonstrated.

We look forward to many years of research with this diffractometer and to a continuing strengthening of the collaboration between JAERI and ORNL scientists.

On behalf of the JAERI participants in this program M.I. would like to express sincere thanks to all the colleagues in ORNL for their hospitality extended to them during their stay in Oak Ridge and also for valuable discussions and suggestions. The technical help by Jim Sellers and his associates is greatly acknowledged.

On the occasion of the first publication of the progress report we would like to express our sincere thanks to Don Stevens of DOE, Mike Wilkinson of ORNL and Yoshikazu Hamaguchi of Muroran Institute for Technology for their efforts to found this cooperative program. Without competent leadership of Ralph Moon at the design and construction stage of the wide-angle neutron diffractometer the present collaborative research would not take shape. Nobu Wakabayashi of Keio University contributed a lot in the discussion and planning of the interesting problems for the research by the diffractometer. Encouragement and administrative help of Kichinosuke Harada was invaluable in pushing forward the activities.

R. M. Nicklow
Solid State Division
Oak Ridge National Laboratory

M. Iizumi
Department of Physics
Japan Atomic Energy Research Institute

II. INSTRUMENT

1. WIDE-ANGLE NEUTRON DIFFRACTOMETER

M. Iizumi, S. Funahashi, S. Katano, Y. Morii,
R. M. Moon, R. M. Nicklow, H. R. Child and M. K. Kopp

I. Introduction

The concept of wide-angle neutron diffractometer(WAND) has been conceived as the principal instrument for the JAERI-ORNL collaboration on neutron scattering at an early stage of the US-JPN cooperation. The conceptual design was started in 1981 and the engineering design took one year from September 1981. The fabrication of the instrument was started from the middle of 1982 and the installation of the instrument at HB-4A of the HFIR was completed at the end of March, 1984. The top view of the wide-angle diffractometer is shown in Fig. 1.

The main objective of the instrument was to utilize the newly developed position-sensitive detector of the curved one-dimensional type with an wide-angle coverage for both the time-resolved measurements of neutron diffraction pattern and also the single-crystal diffraction in the inclination geometry.

This report summalizes the technical part of the one-year experience of utilizing the instrument. This period has been devoted to the performance tests and the demonstration experiments of the instrument. As is usually the case there have been a lot of technical problems to be coped with. The details of these activities are given in separate reports.

II. Performance Test

Since the wide-angle neutron diffractometer is an instrument of the new type consisting of some newly developed parts and aiming at the new functions pointed out above, the performance tests of each part and the instrument as a whole were considered to be quite important to be carried out at the initial stage of the instrument utilization. We spent almost half a year to test the instrument performance and to carry out some

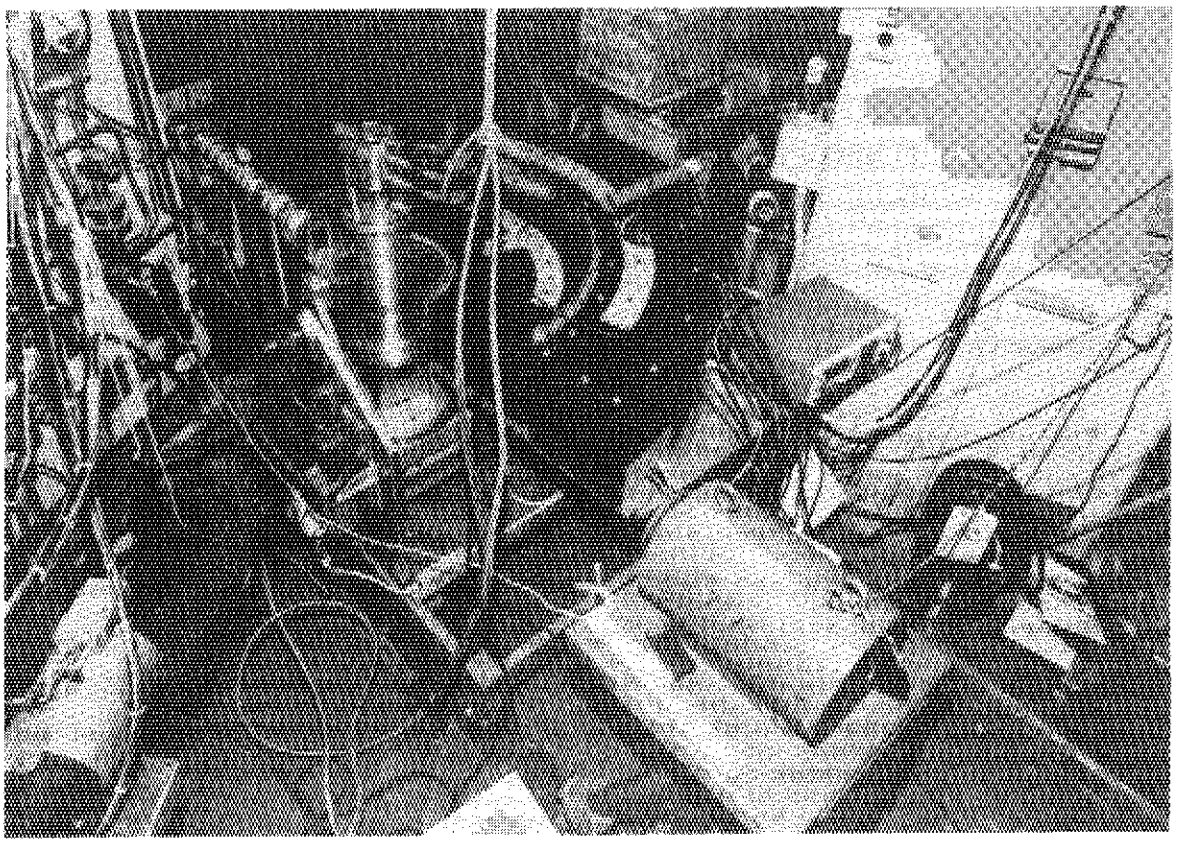

Fig. 1. A oblique top view of the wide-angle neutron diffractometer. The curved one-dimensional position-sensitive counter is inside the black semicircular shielding. A Displex cryostat system is mounted on the crystal table. Neutron beam comes from the top left of the picture through the evacuated beam tube covered with white neutron absorbing materials fixed by bands and through beam narrower and then impinges on the sample on the crystal table.

modification to the instrument based on the findings of the tests. The main test items are as follows.

a. Counter performance

Angular or positional resolution, linearity between the encoded angular value and the true angle, homogeneity of sensitivity and stability of performance of the curved one-dimensional counter were tested and improved.

b. Machine performance

Several motor-driven parts were tested. The collimator drive was adjusted carefully so that the blades of the collimator may not cause any effect on diffraction patterns.

c. Data acquisition and processing system.

The performance of the CAMAC modules such as the time-digitizer and the histogramming memories together with the software system which handles the data acquisition, data transfer to the computer memory, data display, data processing and file management was tested and modified repeatedly in order to adjust to the user's needs.

d. Background

The wide open aperture of the counter gives rise to the background problem more serious than in the case of neutron spectormeters of the normal type. The most harmful source of the background is the air-scattering of the monochromatic beam. The background level was measured and a few measure have been taken to reduce it.

e.Time-resolved measurements.

The time-slicing data acquisition sytem and data handling software were prepared and checked step by step and then the overall performance was tested by actual measurement of the time-dependent process such as the melt of a metal rod and the first-order transition kinetics.

f. Single crystal measurements

The use of the diffractometer for measuring a single-crystal

diffraction pattern on specific layers of the reciprocal lattice was demonstrated for typical examples. Measurements with the tilted counter arrangement were tested.

III. Results of Performance Test

1) Counter Performance. The curved one-dimensional position-sensitive counter developed for this cooperative program by the Instrumentation and Control Division of ORNL is a state-of-the-art product in the respects that it widens the angle coverage to 130 degree keeping a reasonable angular resolution and that a new LC position decoding method is adopted. The required angle-resolution was 0.2 (corresponding positional resolution is 2.6 mm at the counter surface).

The test measurements of the scattered neutron from various samples have disclosed that (1) the linearity between the measured and actual angle is quite good, (2) the resolution of the counter estimated from the full width at half maximum of the neutron peaks measured by placing a cadmium sheet with small holes in front of the counter together with a vanadium rod at the sample position was not so good as it was expected. Although some efforts were made to adjust the high voltage bias applied to the electrodes of the counter and to improve the amplifier performance, the resolution of the counter was still 0.7 to 1.4 degree depending on the position.

More serious about the counter performance is the sensitivity variation as a function of angle. The sensitivity changes from point to point and the sensitivity curve indicates very fine structures fluctuating as much as +50%. This variation was estimated to come from the structure of the electrodes assembly which causes an inhomogeneous drift field and hence no measure could be taken immediately to cope with the inhomogeneous sensitivity. So it was decided to use the counter as it was and correct data for the sensitivity by using the calibration curve obtained from the vanadium rod measurements. Since the stability of the electronic circuit was found not so good as a permanent calibration curve can be used, we are obliged to repeat vanadium runs and obtain the calibration curve from time to time.

With the existing state of the resolution and the sensitivity variation the counter has been used for several measurements without serious difficulty but it certainly limits the utility of the instrument to less sophisticated measurements. So it is highly desirable to make efforts to improve the counter performance.

2) Background. The background counts are still high, though efforts taken up to now were quite effective. The background consists mainly of the neutrons impinging through the front opening of the counter shielding. The air scattering before the sample position was removed substantially by setting a vacuum flight tube. No measure has been taken for the beam path after the sample postion because of the geometrical difficulty. Effectiveness of the moving collimator has been established and the motion was so stable and reliable that it can continuouly be driven for any long run. In order to measure weak scattering such as those from the early stage of nucleation or diffuse scattering from the short-range order, the present background level should be further reduced.

3) Data acquisition system. The data acquisition hardware and software systems have been confirmed to work very nicely. Since the quantity of data acquired for the time-slicing and single-crystal measurements is tremendously large, it has been felt that we are short of both the computer memory and the disk storage capacity.

4) Time-resolved measurements. Feasibility of measuring a fast changing micro-structure depends on how fast one can acquire a single diffraction pattern. The most decisive factor in this respect is the beam intensity which depends on the choise of monochromator. In case of beryllium monochromator now in use we could obtain a diffraction pattern of tolerable quality within one minute. Then we tried actual time-resolved measurements in which micro-structure changes take place in the order of several minutes to several hours.

Two measurements were successfully carried out; both related to the transition kinetics after the temperature is changed stepwisely across the transition temperature. One is the CsCl-like to NaCl-like phase transition in $RbNO_3$ and the other is the transitions between alpha and beta phase in

tin(Sn).

Details are given in a separate report in this progress report. Time-dependent diffraction patterns were recorded by the time-slicing data acquisition system and later analyzed by using several data processing programs which eventually gave the value of the volume fraction already transformed into the new phase as a function of elapsed time. The time-dependence of the fraction was compared with the theoretical prediction based on the classical nucleation and growth theory. In both measurements the transformed fraction was the only one quantity derived from the experimental data. It is desirable to extract the width of Bragg peak in order to get the information with respect to the size of the growing domains. But it was hard to get reliable value of the width with the present degree of the counter resolution.

By these measurements it was demonstrated that the instrument is suitable to carry out measurements of this sort. The microscopic investigation of the kinetics of the first order transitions is one of the most undevloped and very promising problems in the statistical physics. The wide-angle neutron diffractometer is going to be a unique research tool in this field.

5) Single crystal diffraction. Efficient measurements of the diffraction from single-crystal specimen was demonstrated by using a few samples. After collecting a large number of diffraction patterns each corresponding to a successive angle of crystal rotation, a data processing program displayed the intensity maps on a plane of the reciprocal space. Measurements with the flat-cone method was carried out successfully by tilting the crystal table and counter assembly.

The measurements of the single crystal diffracion indicates that it is promising to use the instrument for the single crystal diffraction of the incommensurate systems. Effective observation of diffuse scattering is one of the purpose of the single crystal diffraction by the WAND. Unexpectedly clear observation of the thermal diffuse scattering in CuAlNi sample suggested that the diffuse scattering measurements are also very promising. In order to take full advantage of this instrumental capability it is indispensable to have a good software system for displaying and processing data. The prelimianry system has been improved and replaced by

more sophisticated systems.

IV. Remaining Problems

1) Monochromator. Right now we are using a beryllium monochromator crystal, provided by the Chemistry Division, together with the old monochromator drive system. The initial plan was to make available a distorted silicon monochromator and another auxiliary monochromator and to mount them on the new drive mechanism. This plan has not been realized because a good silicon monochromator has not been available and the new monochromator drive system has had some troubles in the motor drive. Some efforts to produce a silicon monochromator is underway in JAERI as described in a separate report. It is highly desirable to increase the beam intensity by factor of five to ten to measure faster kinetics or weak diffuse scattering.

2) Counter. As described earlier the counter has some drawbacks such as the medium resolution and inhomogeneous sensitivity. It will be necessary to improve the counter performace before we can use WAND in more sophisticated problems. Remodeling of some essential part of the counter may be necessary in future.

3) Data Aquisition System. The connection to the main frame computer has not been fully exploited for data-processing by the large computer system. A special Rietveld type program should be prepared for processing time-resolved data. The data transfer to the JAERI laboratory is another problem to be resolved in near future.

2. PERFORMANCE OF THE CURVED PSD

H. R. Child

The detector for the new machine consists of a curved position sensitive proportional counter using position encoding based on the shape of the neutron pulse obtained from each end of the detector. Due to the distributed inductance (L) and capacitance (C) of the anode-cathode configuration of this detector, the pulses from a single neutron detected along the arc of the detector have different shapes at each end of the detector. The time at which these pulses after amplification cross the base line, the so-called crossover time, is used as a measure of the pulse shape and the time difference between these crossover signals from each end is proportional to the distance along the arc of the detector. These time signals start and stop a CAMAC time digitizing converter module (TDC) which generates a digital address from them and adds a base address offset, and this resulting address is provided on an external bus to a histogramming memory. The memory increments the address to record the neutron event. Several memories (currently, we have three) containing 16 k 24 bit words each are on an external address bus so data can be shifted easily into different memory regions by simply changing the base offset address. Thus, while a data run is being accumulated, no computer time is needed for the data acquisition process. Furthermore, data can be copied from the memories via the CAMAC dataway even while the data are being accumulated so that a run can be examined before completion.

A time resolution in the TDC of 0.625 nanoseconds/channel has been found to give 0.1° per channel and approximately 1300 channels of usable data per run. We use regions of 2048 channels of memory and fit this active range into these regions. Thus, eight runs can be accumulated in each memory module. The linearity of the detector is measured by measuring a pattern from Ni powder whose Bragg peak positions are accurately known for a given wavelength. The observed channel numbers for the peaks are least squares fitted to the calculated scattering angles by a linear form and the coefficients stored with the data runs to convert from channels to angle along the arc. The linearity in angle along the arc vs channel is very good. Two polynomial coefficients fit the observed peaks in all cases

and if a third coefficient is tried in the fit, it turns out to be zero within its error. The angular resolution of the detector alone is difficult to measure, but we find about 0.9° FWHM near the center.

The scattering from vanadium which should be constant with scattering angle is measured and a sensitivity correction factor, i.e., a multiplicative factor as a function of channel which yields a constant scattering is calculated from the vanadium data and used for other sample runs. This sensitivity varies from channel to channel showing a great deal of structure and varies by 50% at some spots. Obviously, the sensitivity must remain constant if data are to be trusted so the sensitivity is measured often and comparisons made. The figure shows a portion near the middle channels of three sensitivity correction runs made over a four-month interval and the structure is well illustrated. The stability is also shown by the fact that the three runs agree within the statistical error. This sensitivity variation is presumed to reflect inhomogeneties in the internal electric fields in the detector. A second detector is being built, and it will be interesting to see if it shows a more uniform response. If so, perhaps a decision can be made concerning what should be done to correct this problem.

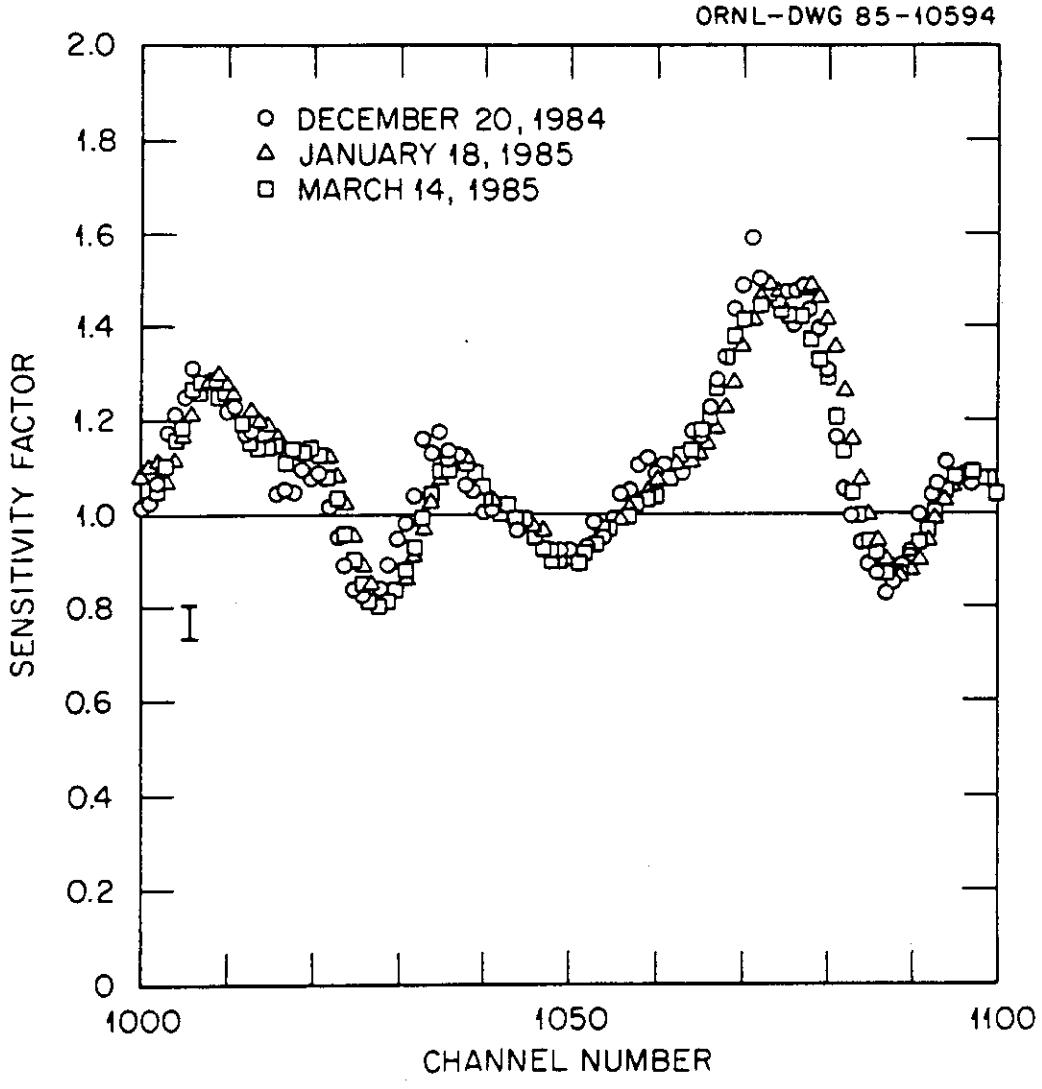

Fig. 1. Sensitivity factor vs channel near the center of the detector over a three-month time interval.

3. SOFTWARE

H. R. Child

The computer which controls the WAND machine is a Digital Equipment PDP 11/44 with 512 kilobyte of internal memory and four RL02 10.4 megabyte disk drives. It is connected to a CAMAC system which controls data acqusition and to a Smartstep motor driver and power supply which drives the motors used for positioning. A DECwriter, three CRT VT100 type terminals, and a Tektronix 4114A plotting terminal are connected for I/O. In addition, a telephone line and modem allows transmission of data to the Laboratory's large central computers. The operating system is the RSX11M multiuser, multitasking system DEC provides. The programs for acquiring data and data analysis were locally written in the fortran 77 language. The data acquisition program has capabilities for time slicing (both periodic and nonperiodic) and scanning in which data are accumulated as one or more motor positions are stepped. The data runs are saved in a form usable to the data analysis routines on the disks. Individual data runs can be corrected for background and/or sensitivity, normalized, nonlinear least squares fitted, and plotted in whole or in part on line. Sets of data can be examined to show what regions of reciprocal space were measured with a relative indication of the intensity distribution in the region. This latter capability was necessary to visualize the complex distribution of the data with this flat cone geometry machine which takes data simultaneously over a curve in reciprocal space which depends on many variables.

4. DATA PROCESSING IN SINGLE CRYSTAL DIFFRACTOMETRY

S.Funahashi, H.R.Child and S.P.King

The wide-angle neutron diffractometer has very big capabilities not only in the high speed polycrystalline diffraction measurement but also in the single crystal diffractometry. It can be easily done to collect diffraction intensity of a certain reciprocal plane which is parallel to the equatorial plane except the so-called blind area. This kind of measurement makes it possible, for example, to detect satellite reflections or streaks which are otherwise often missed.

The principle of the flat-cone single crystal diffraction geometry of the WAND and an outline of the software to display the single crystal data are described in the following sections.

1. Flat cone geometry.

The WAND machine is equipped with the following mechanisms to meet the flat cone diffractometry requirement. (1)The sample goniometer is mounted on the counter table which holds the wide-angle counter. The central axis of the sample goniometer is set perpendicular to the counter table and the goniometer is turned about this axis by the program. We define the turning angle of the sample goniometer as ω. (2)The counter table can be tilted, with the sample goniometer on it, about the horizontal axis which passes through the sample positition and is perpendicular to the incident beam. We define the table tilt angle as TTILT.

We define another angle η which designate the direction of a scattered neutron on the counter table plane. This angle η directly corresponds to the position or the channel number of the wide-angle counter. The direction of the incident neutron beam when the counter table is set flat is taken as the origin of the η-angle.

Figure 1 schematically shows the ω-, η- and TTILT-angles. In this figure, the arc between the points A and B represents the sensitive region of the wide-angle counter. The point D is the position which falls on the neutron beam line when the counter table is set flat(i.e. TTILT=0). The

point S means a single crystal which is to be turned about the ω-axis. Regarding the sample, we assume the lattice parameters to be a, b , c, α, β and γ as usual.

To start with, we take the case that the counter table is set lat (i.e. TTILT=0). Figure 2 shows the reciprocal plane and the incident and the scattered neutron wave-vectors k_0 and k_f. We take SPV vectors $[h_1,k_1,l_1]$, $[h_2,k_2,l_2]$ and $[h_3,k_3,l_3]$ to specify the crystal orientaion. Here, h_1,k_1,l_1 etc. mean the sets of Miller indices based on the reciprocal vectors a*,b*,c*. We assume that $[h_1,k_1,l_1]$ and $[h_2,k_2,l_2]$ are lying on the counter plane. As the home position, we choose the configuration that $[h_1,k_1,l_1]$ is parallel to the incident neutron beam and here we assume $\omega=\omega_0$(ZERO angle of ω). The third SPV $[h_3,k_3,l_3]$ is assumed to be pointing upward.

The geometrical configuration of these vectors and angles are illustrated in Fig.2(a). At one measurement (called as one scan) we measure neutrons scattered between A and B in Fig.1. This counter region corresponds in the reciprocal space to the arc A'P'B' which is a part of a circle centered on C as shown in Fig.2(b). When the sample is turned with the goniometer, the reciprocal lattice is turned relative to the neutron beam and the counter system about an axis which passes the origin O and is perpendicular to the basal plane defined with $[h_1,k_1,l_1]$ and $[h_2,k_2,l_2]$. It is easier to understand, however, to consider that the reciprocal lattice is fixed and the system of the neutron beam and the counter is turned relative to the reciprocal lattice. Eventually, the counter scans the basal plane turning the arc about the origin O as shown in Fig.2(b).

In general cases, the counter table is tilted. As shown in Fig3(a), we consider the incident neutron wave-vector k_0 is tilted relative to the basal plane instead of considering that the reciprocal lattice is tilted. Fig.3(a) shows the home position described above, and the arc A'P'B' lies on the plane O' which is parallel to the basal plane defined with $[h_1,k_1,l_1]$ and $[h_2,k_2,l_2]$. When the sample is turned about the central axis of the goniometer, the arc scans the O'-plane as shown in Fig.3(b). In this case, the area enclosed with the circle is called the blind area where we cannot reach with this configuration.

2. Calculation and Graphic programs.

As described above, the neutron diffraction intensity of a reciprocal plane required can be collected with the WAND by turning the sam at a fixed TTILT-angle. Since a little complicated calculations and d processing procedures are needed to make good use of the WAND, some computer programs have been prepared for the users. The number of the data points are so large that the system is only effective when the data are displayed as a two-dimensional figure. In the present case, however, there is no standard two-dimensional perspective graphic subprogram available for our purpose because of two reasons, i.e. the data points are not distributed with equal intervals on the reciprocal space and the number of the data are too many. The INMAPB and INMAPV programs are developed to display the data intensity with the marker of the Tektronix 4114 or with other modes. Other useful programs for the users are MAINSA and RECMAP. The main features of the functions of these programs are described below. The detailed instructions to use them is either given in other place or can be told by the person who is responsible for the instrument operation.

(1) MAINSA: This program calculates some numerical informations concerning the ω-, η- and TTILT-angles as well as reciprocal coordinates. This program has two functions. The first is that the user can get the ω-, η- and TTILT-angles by inputting the reciprocal lattice coordinate(Q). The second function is the inverse of the first, i.e. the user can obtain the reciprocal coordinate by inputting the ω-, η- and TTILT-angles. It is necessary for the users to input the lattice parameters, the neutron wavelength and SPV's at first. Then the calculation is straightforward.

(2) RECMAP: In principle, this program is quite similar to the MAINSA program described above and has the additional graphic display function. This program draws curves like those shown in Fig.2(b) on the Tektronix 4114 screen. A guide to use this program is stored on the disk DL0:[3,3] as RECMAP.MAN.

(3) INMAPB and INMAPV: These two programs display the measured diffraciton intensity on the Tektronix 4114 screen. These programs have many functions to make the map easy to be understood. For example, the map can be enlarged, rotated, translated, reduced etc. It is also possible for the user to read the reciprocal lattice coordinate on the screen by making use of the cross-hair cursor. The coordinate can be given in the SPV unit as

well. The counter sensitivity correction can be done if it is requested. Since the lattice parameters, the wavelength and the ω-, η- and TTILT-angles are stored in the experiment header and the scan headers, it is not necessary for the user to input them again. It is, however, possible for the user to change the parameters or to add any correction to them in these programs*. Figure 4 shows a typical example drawn by INMAPB program of data taken of a Cu-Al-Ni alloy single crystal at TTILT=0 position with $[h_1,k_1,l_1]=[2/3,2/3,0]$ and $[h_2,k_2,l_2]=[-2/3,2/3,0]$. The diffraction intensity is classified into ten grades of darkness. The three figures in Fig.4 show the same data with different darkness. Horizontal streaks are observed between the strong Bragg reflection spots. Figure 5 shows another typical diffraction map of data taken of a single crystal of Rb_2ZnBr_4 at a tilted counter table configuration(TTILT=15°). SPV's are [100], [001] and $[0\bar{1}0]$. At the present TTILT angle, the point O' is $0\ \bar{2}\ 0$ and the map shows the k=-2 plane. The center of the rectangle in the left figure is, therefore, $5\ \bar{2}\ \bar{2}$. The right figure is the enlarged map of the area enclosed in the rectangle. Numbers of satellite reflections are observed on the vertical lines which are indexed as $h\ \bar{2}\ \ell\pm\delta$. Diffraction points are a little spread on this plane due partly to the counter resolution and partly to the big size of the sample.

In order to save the computer memory space, INMAPB reads only one scan data at a time and draws a curve before it reads the next scan into the same memory place. On the other hand, INMAPV can read up to 30scans X 140channel data at a time and keep them. This size can be changed by changing only two parameters in the program, but a bigger data area will sometimes cause troubles in the time sharing. If the computer had a bigger memory place to store numbers of scan data at a time, the drawing could be done a little quicker than done with INMAPB and it would be done by far the quicker in the case of redrawing the same data after any modification.

---

* An instruction for the users is stored on the disk DL1:[31,31] as INMAPB.MAN.

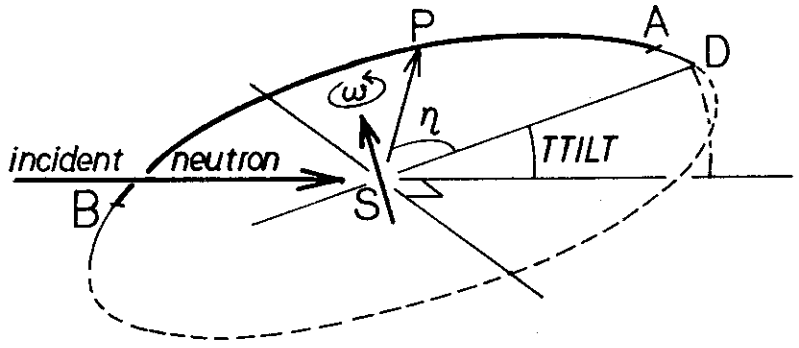

Fig.1 Schematic picture of flat-cone geometry in real space. Arc APB indicates the sensitive area of the wide-angle counter. Definition of the angles ω, η and TTILT are described in the text.

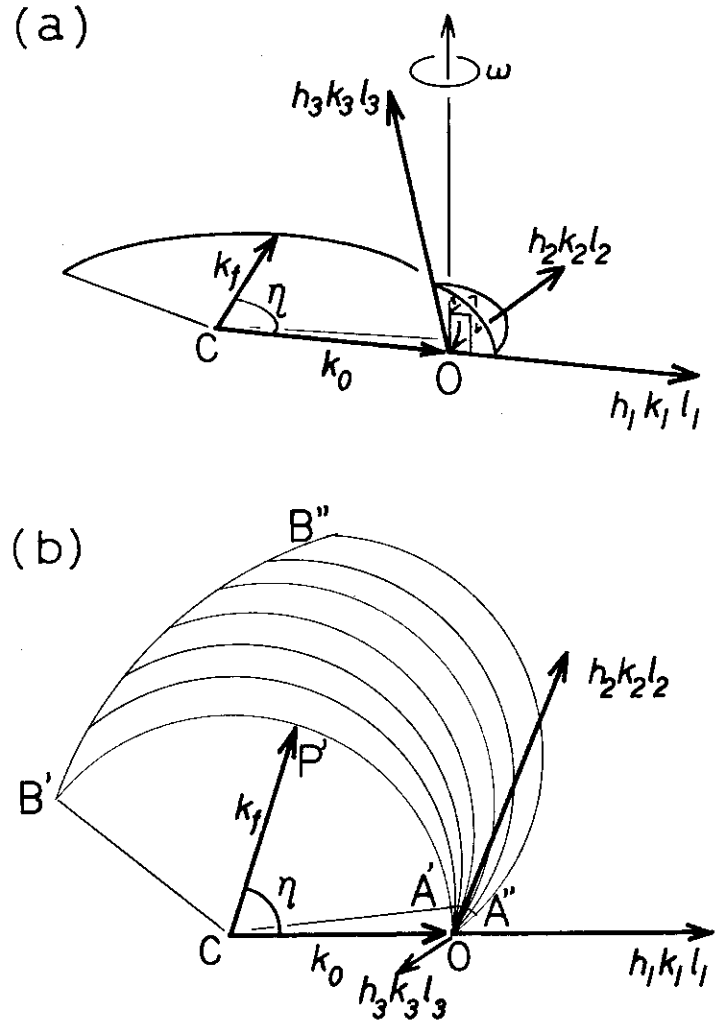

Fig.2 Schematic picture of the configuration of the reciprocal lattice and the incident and the scattered neutron wave-vectors for the case of TTILT=0. (a)Perspective at home position. (b)Plan. Arc A'P'B' corresponding to APB in Fig.1 scans the plane as shown here when the sample is turned.

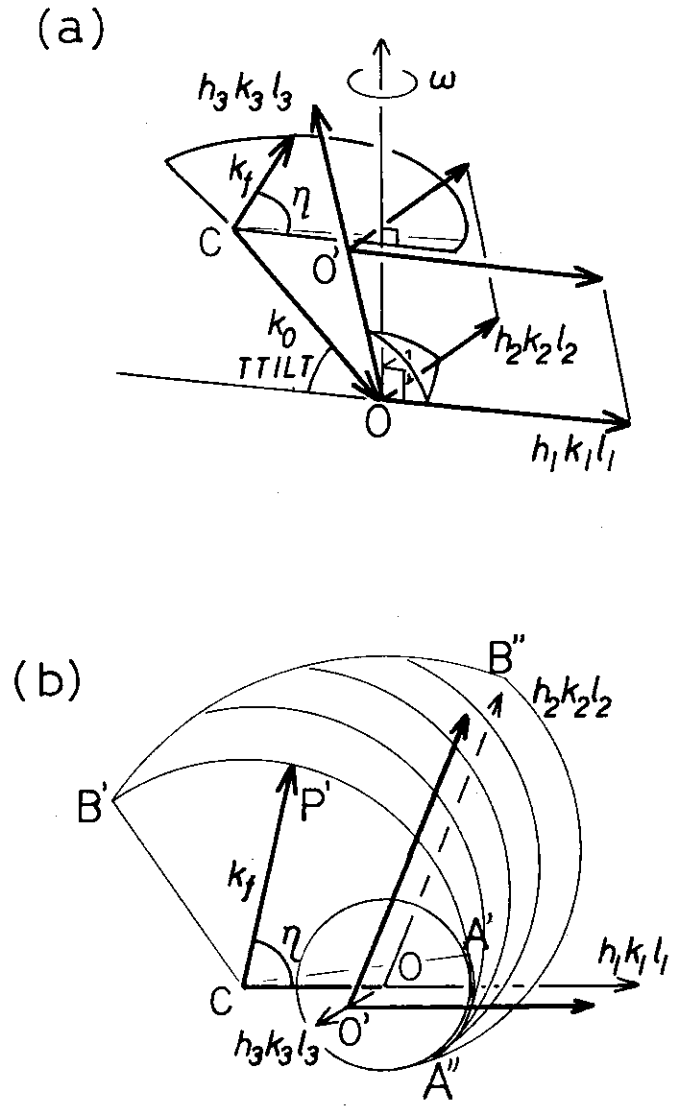

Fig.3 Schematic picture of the configuration of the reciprocal lattice and the incident and the scattered neutron wave-vectors for the case that the counter table is tilted. (a)Perspective at home position. (b)Plan. Arc A'P'B' corresponding to APB in Fig.1 is lying on the O'-plane and scans the plane as shown here when the sample is turned.

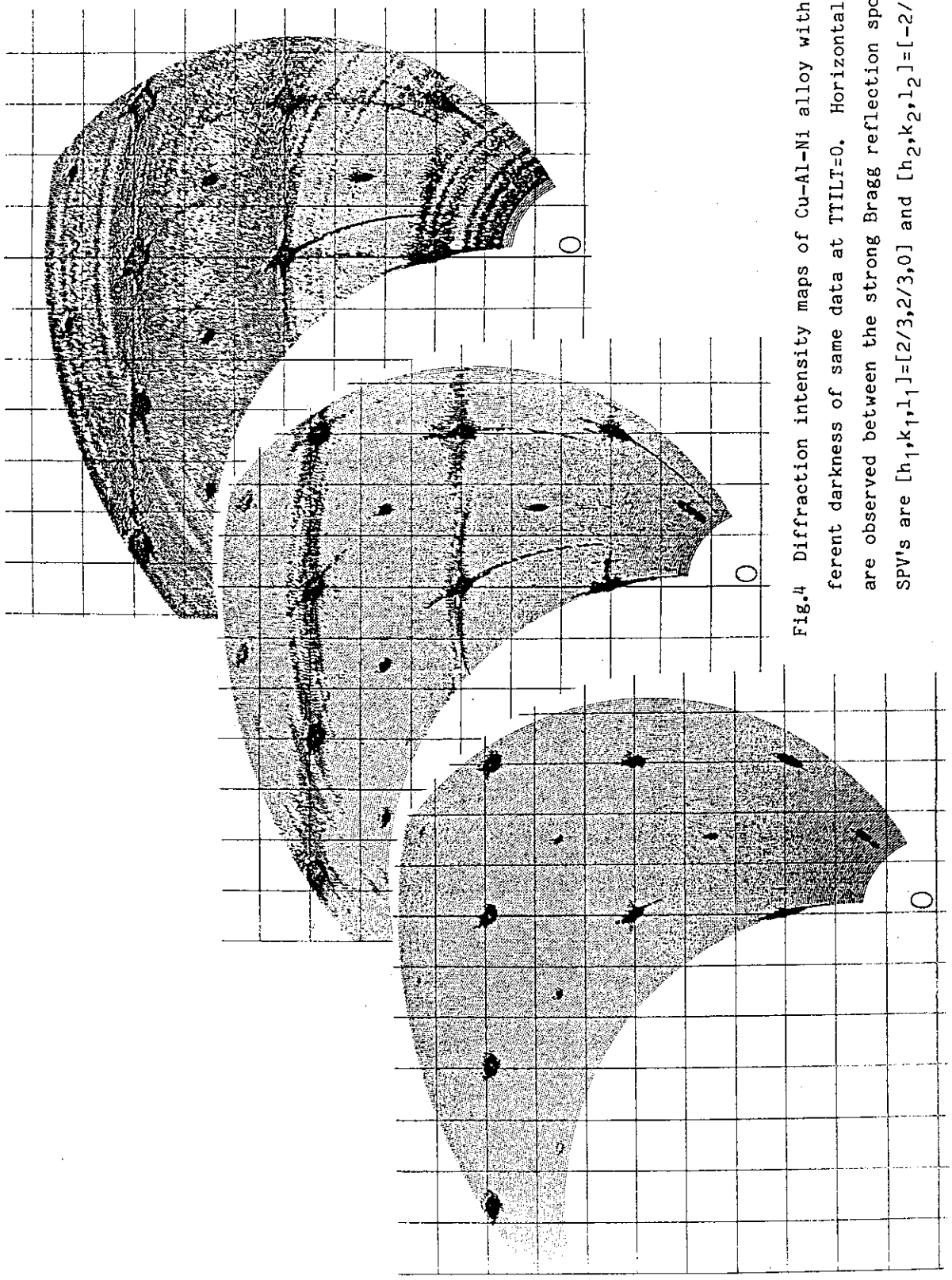

Fig.4 Diffraction intensity maps of Cu-Al-Ni alloy with different darkness of same data at TTILT=0. Horizontal streaks are observed between the strong Bragg reflection spots. SPV's are $[h_1,k_1,l_1]=[2/3,2/3,0]$ and $[h_2,k_2,l_2]=[-2/3,2/3,0]$.

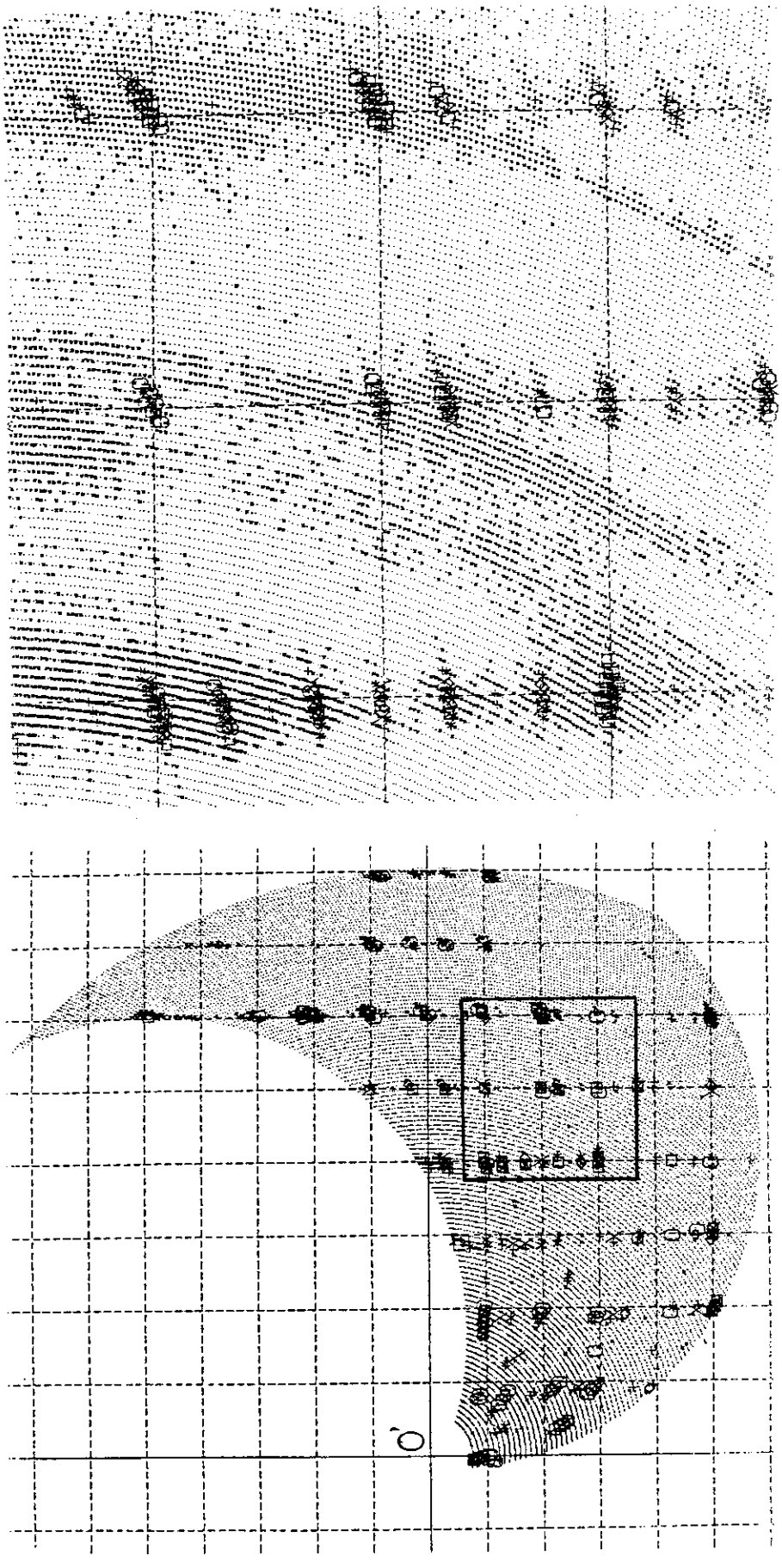

Fig.5 Diffraction intensity map of Rb_2ZnBr_4 at a tilted counter configuration(TTILT=15°). SPV's are [100], [001] and [0$\bar{1}$0]. The net-plane shows k=-2 plane. The right figure shows the enlarged map of the area enclosed in the rectangle in the left figure.

5. FURNACE FOR RAPID CHANGE OF TEMPERATURE

S. Katano, H. Motohashi and M. Iizumi

Real-time experiment of time-dependent phenomena is one of the most interesting research subjects of the wide-angle neutron diffractometer installed in HFIR, since this diffractometer is able to obtain a diffraction pattern all at once. At high temperatures, we have good examples of these time-dependent phenomena: first-order phase transitions such as order-disorder transition, phase separation and so forth. For these experiments, it is desired to change the temperature of a sample as rapidly as possible. Therefore, we fabricated a new-type furnace which is able to control the temperature-change at a very high rate.

This furnace makes use of circular infrared-lamps for rapid heating and high pressure gas-blows for rapid cooling. A schematic drawing of the furnace is shown in Fig. 1. A sample (A) is mounted on a holder (B) made of transparent quartz. These are placed in a quartz tube (C) of diameter 80 mm whose inside can be evacuated. The heating element is a pair of circular infrared-lamps (D) over and under the sample. The neutron beam can go through the reflector (E) made of aluminium alloy 2 mm in thickness. The inside-surface of this reflector was coated with gold. To get a high-heating rate and wide uniformity of the sample temperature, this reflector roughly focuses images of the lamps on the sample. For a rapid-cooling, the high pressure gas blows against the sample from many small holes of two rings (F) made of quartz. This gas-blow is controlled by valves (G). The sample-temperature was measured by two chromel-alumel thermocouples; one of them was welded on the surface of the sample and the other was placed in a hole made near the center in the diametrical direction of it. The temperature of the sample, the rate of the temperature-change and the operation of gas valves are controlled by a programmable temperature controller.

The result of a test which was intended to get the rate of $\pm 1000^{\circ}C/min$ between 200°C and 800°C is shown in Fig. 2. As the sample, a stainless steel rod 10 mm in diameter and 30 mm in length was used. For the temperature control, the thermocouple welded on the surface of the sample was connected with the temperature controller. In this figure, the straight line shows the time dependence of the temperature on the surface and the dash-dotted line

does that near the center. The heating up to 800°C was done by putting of the power on the heaters, and the cooling was done by cutting it and simultaneously by blowing the high pressure gas of about 5 kg/cm^2. The result shows that the heating rate of 1000°C/min can be easily obtained. The difference of the temperature between the surface and the inside was not observed. In cooling, the obtained cooling rate was about -800°C/min at the beginning, -550°C/min around 600°C and -300°C/min around 400°C, and the temperature-difference between the surface and the inside was clearly observed. For reference, the result of the cooling without the gas-blow is shown by the dashed line.

Figure 3 shows the result of repeats of the rapid change of temperature. The case of the temperature-change between 600°C and 400°C is shown in (a) and that between 495°C and 500°C is in (b). In the latter case, a continuous gas-blow at about 1 kg/cm^2 was needed to obtain a good stability of temperature.

Using this furnace and the wide angle neutron diffractometer, the relaxation process of the order-disorder transition in CuZn and Ni_3Mn alloys was investigated: near the critical temperature, the decay of the superlattice peak in the ordered state and the growth of the short range order (SRO) in the disorded state were studied. It is well known that CuZn exhibits the second-order transition. Thus, it is considered that the time constant is quite short. However, the experiment by electrical resistivity indicated that the time constant of growth of SRO at about 5 degrees above the transition temperature is over one hour.[1] If it is correct, this process is easy to observe. Figure 4 (a) shows the time dependence of the (111) superlattice peak after the temperature was increased from 450°C to 465°C. (The transition temperature is around 470°C.) In experiments, a sample of 5 mm diameter was used. The insert shows the temperature-change of this sample. Although temperature reaches to the desired temperature in a few seconds, after then it oscillated. However, the temperature became stable in about 15 seconds. The time-resolved experiment for 10 seconds was done until 5 minutes passed. To get good counting statistics, this measurment was repeated 120 times and each of data for 10 seconds was accumulated in the memory outside the computer. For reference, the diffraction patterns at 450°C and 460°C at the equilibrium state are shown in the figure. The integrated intensity of these peaks is shown as a function of time in Fig. 4(b). From these figures, it is found that the superlattice peak and its intensity saturate within 5 seconds: the time constant is very short. The experiment for the growth of SRO investigated

by the change of the temperature from 550°C to 475°C also shows that the time constant is quite short. Although the difference between this and the electrical resistivity measurement is not clear at present, the result obtained here seems to be reasonable if we refer to the neutron diffraction study on SRO of this alloy; SRO peak was distinctly obtained in a quick scan of the total time of 90 minutes.[2)]

The result on (211) peak of Ni_3Mn is shown in Fig. 5(a) and (b). The temperature was increased from 470°C to 490°C. (The transition temperature is around 510°C.) It is known that the transition of this alloy is the first-order and the time constant is fairly long.[3,4)] Thus, the time-resolved measurement for 10 minutes was done until 12 hours passed. As shown in these figures, it is clearly observed that the superlattice peak decays with time. The obtained time constant is about 30 minutes. This result is consistent with the previous reports though the value is somewhat shorter than theirs. The growth of SRO was investigated by the change of temperature from 600°C to 515°C. Since the intensity is small and broad, the counting statistics was not enough. However, the result indicates that the time constant is over 10 minutes.

In conclusion, the rapid-temperature change can be stably obtained by this system. If we use a smaller sample, the higher rate of the temperature-change can be attained. Using this furnace with the wide angle neutron diffractometer, it is possible to do real-time experiments of time-dependent phenomena with a time constant of over 30 seconds.

References

1) I. Hatta and M. Shibuya: J. Phys. Soc. Jpn. 45 (1978) 487.
2) C. B. Walker and D. T. Keating: Phys. Rev. 130 (1963) 1726.
3) M. R. Collins and H. C. Teh: Phys. Rev. Lett. 30 (1973) 781.
4) N. Wakabayashi: unpublished.

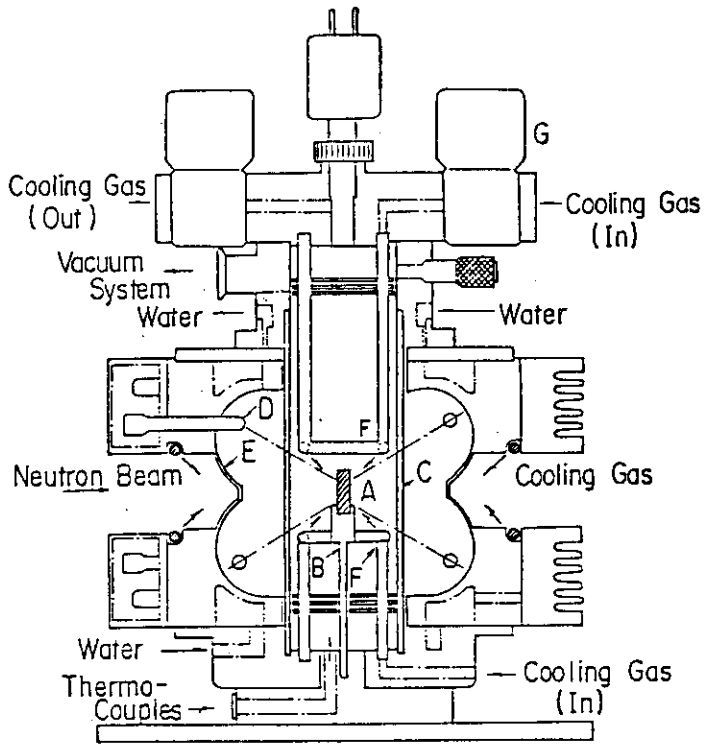

Fig. 1. Schematic drawing of the furnace: A - sample; B - holder; C - quartz tube; D - infrared-lamp; E - reflector; F - ring for gas blow; G - valve for high pressure gas.

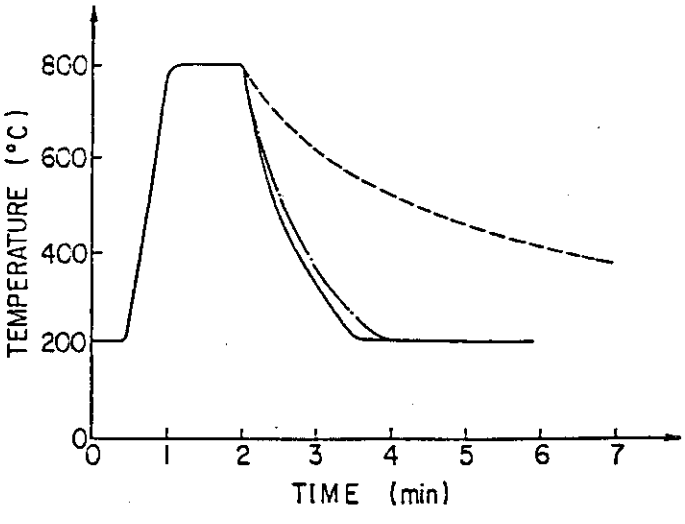

Fig. 2. Time dependence of temperature. A stainless steel rod 10 mm in diameter was used. The solid line shows the temperature measured on the surface of the sample and the dash-dotted line does that near the center in a diametrical direction of it. The dashed line indicates the result of the cooling without gas-blow.

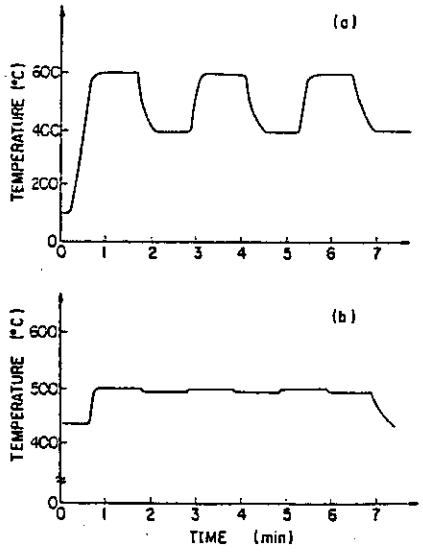

Fig. 3. Time dependence of temperature when the rapid temperature-change was repeated: a - between 400°C and 600°C; b - between 495°C and 500°C.

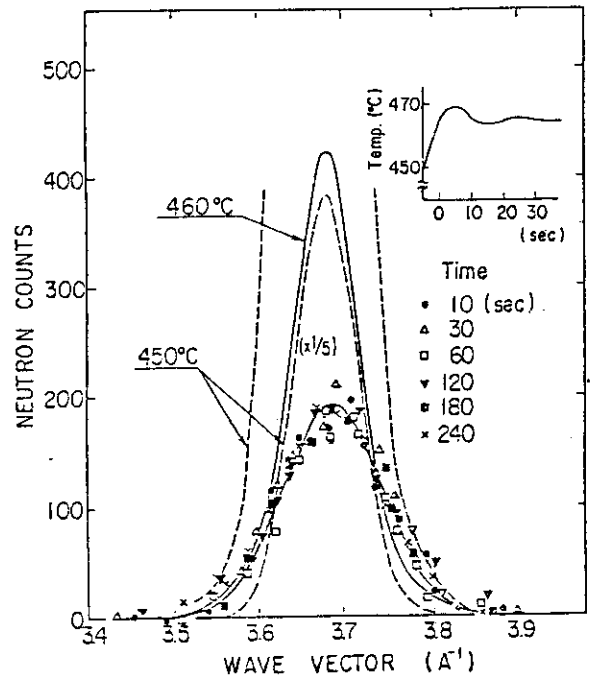

Fig. 4(a). Time dependence of the superlattice peak of CuZn when temperature was changed from 450°C to 465°C. (The transition temperature is around 470°C.) The insert shows the temperature as a function of time.

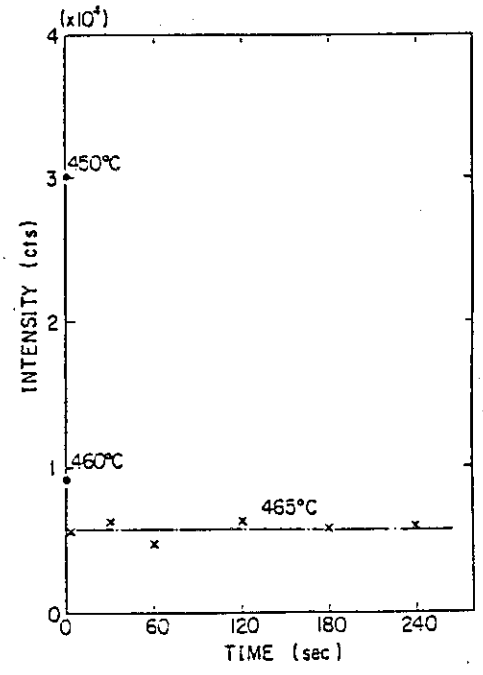

Fig. 4(b). Integrated intensity of the superlattice peak of CuZn as a function of time.

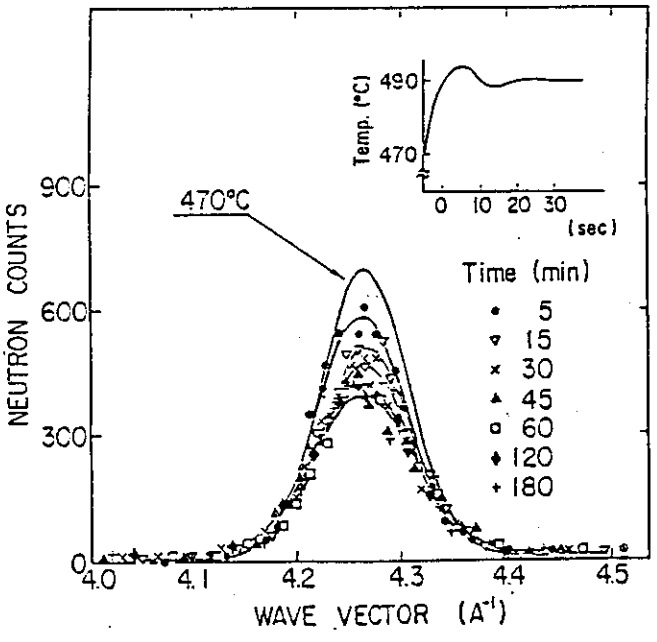

Fig. 5(a). Time dependence of the superlattice peak of Ni_3Mn when temperature was increased from 470°C to 490°C. (The transition temperature is around 510°C.) The insert shows the temperature as a function of time.

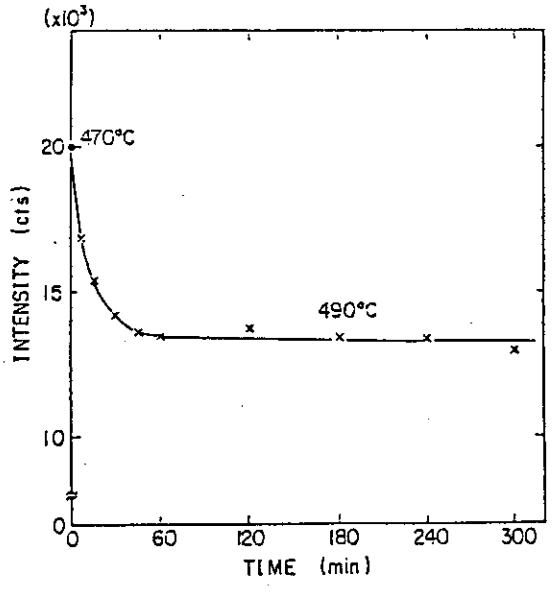

Fig. 5(b). Integrated intensity of the superlattice peak of Ni_3Mn as a function of time.

6. STRESS-MODULATION MACHINE

Y. Morii, N. Minakawa, and M. Iizumi

The stress-modulation machine was installed and tested as an auxiliary equipment of WAND in April 1985. The machine provides 1 ton-force uniaxial stress in either static or dynamic mode and high temperatures up to 800°C for the study of stress-induced phase transitions.

Load unit is shown in the figure. Experimental specimen was set in the center of inside of the sample chamber (1), and the servohydraulic actuator (7) driven by a stress controller (not shown in the figure) regulates oil pressure to apply programmed stress in the mode of either compression or extension on the specimen through the piston rod (3). The dynamic stress such as sine, triangle, square waves and step-like change were demonstrated. The stress was measured by the load cell (6) and fed back to the stress controller. The stability of the stress was less than ±1% of full scale of setting. Stress can be driven by an external function generator as well as by an internal one so that it will be allowed for us to synchronize stress-modulation with the neutron data acquisition system in time-resolved experiments.

Furnace consists of cylindrical shaped molybdenum heater and three thermal shields which surround the sample. Low electric voltage (up to 5 volts) and high currents (up to 400 amperes) were sent by a programable temperature controller (not shown in the figure). Temperature fluctuation was turned out to be only ±2°C at 800°C over the 40-mm long rod sample with 10-mm diameter.

Since the sample chamber was designed as not only a vacuum shield but also as a part of load frame, number 5062 aluminum material was used to be machined out 2.5-mm thick window for neutrons.

The stress-modulation machine is designed to be utilized for the studies on kinetics of stress-induced phase transitions in CuAlNi, MnNi, and MnCu alloys and on magnetoelasticity in MnNi and so on.

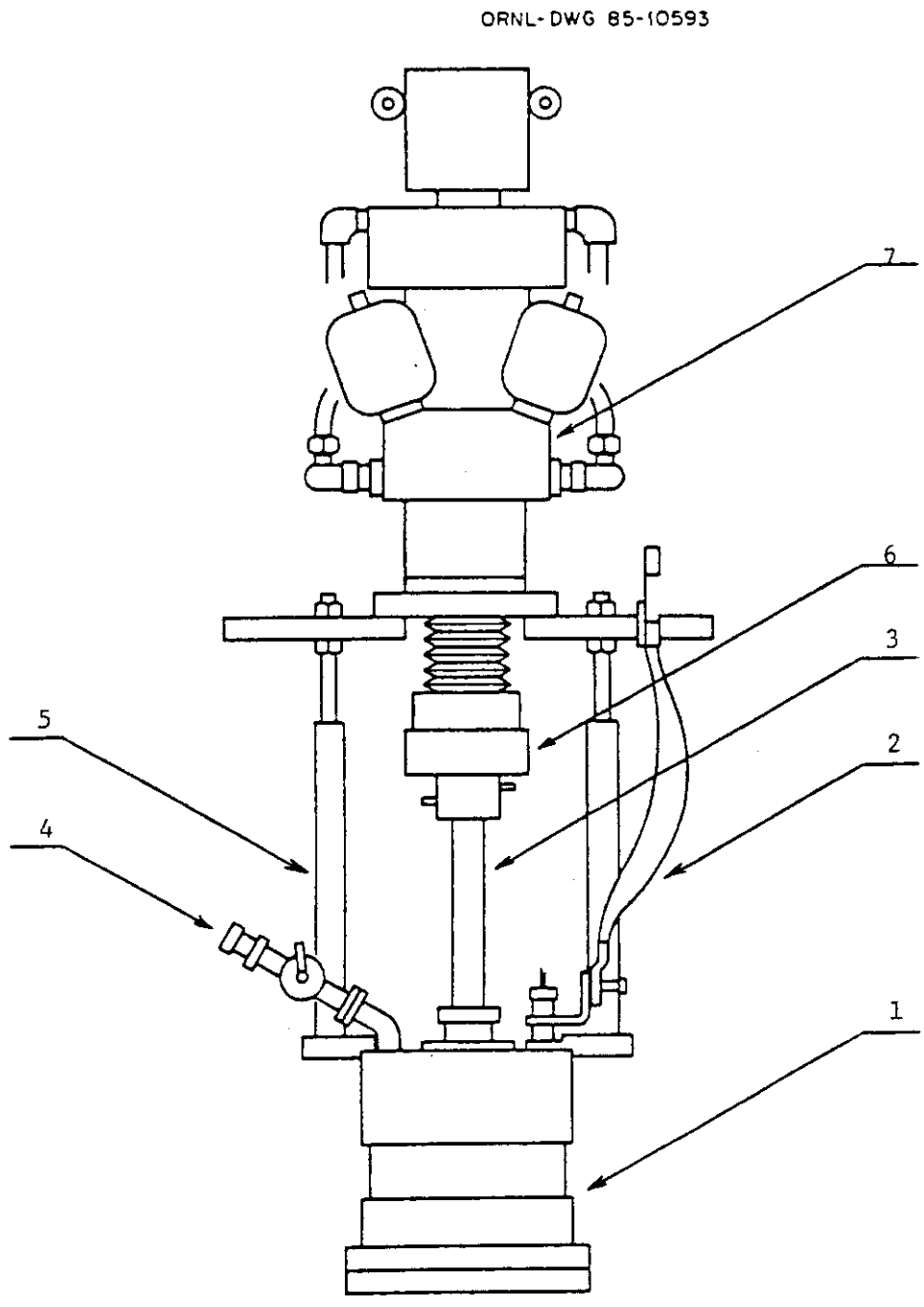

Fig. Load unit of the stress-modulation machine.
1: Sample chamber, 2: Heater current leads,
3: Piston rod, 4: Pumping line, 5: Load frame,
6: Load cell, 7: Servohydraulic actuator.

7. Monochromator Improvement

S.Funahashi and N.Minakawa

Monochromators of high reflectivity for reasonable wavelength are strongly needed for WAND. As the monochromator take-off angle is fixed at 52.5°, it had been planned to install two monochromator goniometers in order to make it possible to choose suitable wavelength according to the experiments. Unfortunately, it is only the beryllium monochromator of the chemist group which is available at present. The Be 110 reflection gives a good beam at about 1Å wavelength, but the intensity is rather poor. In addition, this wavelength is too short for most experiments of WAND considering the rather poor angular resolution and the wide angle range of 130° covered with the counter. The reflections of Be 100(λ=1.75Å) and 101 (λ=1.53Å) are good from the standpoint of the wavelength, but not a negligible half wavelength contamination puts another problem.

In order to provide effective monochromators for convenient wavelengths, it is being attempted to make use of a set of sliced silicon plates assembled in a mechanically bent form. Silicon 113 plane (d=1.638Å) was chosen as the reflection plane because the wavelength of 1.45Å at $2\theta_M$=52.5° is reasonable and the second order reflection is absent.

Thin plates of two different thicknesses of 0.5 and 0.15mm were tested. Since the raw material was a perfect crystal rod of 7.5cm diameter and the rod axis was parallel to the 111 axis, the plates were elliptic with the minor axis of 7.5cm. An assembly of plates was placed to an aluminum holder which has a circular hole of 7cm diameter. The assembly was pushed toward the holder with an aluminum rod at the center of the back side of the assembly. The effect of bending the assembly was measured with a conventional triple axis spectrometer installed to JRR-2 reactor of JAERI. Geometrical configuration of the measurement is shown in Fig.1(a). The assembly was put at the sample position. The wavelength used was 1.41Å because the scattering angle was set about 51° which is close to the monochrometer of WAND(52.5°). The preliminary results are as follows.

(1)Rocking curves. Fig.2 shows rocking curves measured of a single plate of 0.5mm thickness with the change of the bending. Parameter Δ is

the displacement of the center of the plate as shown in Fig.1(c). The θ-2θ scannings were also carried out but only a slight increase of the line width was observed with Δ. The collimators of this measurement were all 30'. This collimation is larger than that of the WAND beam. Therefore, it is the peak intensity of Fig.2 that is meaningful. The maximum peak intensity is attained between Δ=0.2 and 0.3mm. The peak height of the case of Δ=0.2mm is about 2.4 times that of Δ=0.

(2)Thickness. (a)Without the bending a ten plate assembly showed an intensity of about ten times as large as that of a single plate. But the maximum reflectivity observed at Δ=0.25mm was about 1.5 times of the reflectivity at Δ=0. (b)Without the bending the reflectivity of a single 0.15mm plate was much higher than that of 0.5mm plate, but the maximum reflectivity obtained by the bending was nearly equal for the two thicknesses.

(3)Optical effect. The result of Δ=0.6mm in Fig.2 shows a splitting of the diffracted beam indicating optical effect of a concave reflecting plane. In order to check this phenomenon, photographs were taken at the positions indicated in Fig.1(b). Some of the typical pictures are shown in Fig.3. The photograph at L=151cm and Δ=0.3mm shows a clear image of the second collimator. The photographs of Δ=0.6mm show focusing at shorter distance and defocusing at L=151cm. Here, L is the distance between the silicon assembly and the camera.

(4)Comparison of intensity. Though absolute intensity has not been measured, comparison with a flat P.G. may give some measure of the intensity. The intensity measured with 0.5mmthick×10plates with Δ=0.25mm was about 1/10 of that measured of an assembly of a 1"×2" P.G. at the same wavelength(i.e. 2θ=24.3°).

The increase of the reflectivity with the bending is due presumably both to the decrease of the primary extinction and to the focusing effect. If we assume the plate is bent spherically, the displacement of Δ=0.25mm at the center of 7cm diameter circle gives a radius of 245cm or a focal distance of 123cm. The effective distance between the silicon reflecting plane and the counter via the analyzer along the normal of the reflecting plane(b) is about 54cm*. If we take into account the fact that the

* $(60+66)\times\sin(51°/2)=54$

monochromator in this experiment is a curved P.G. of which focal distance is 39.4cm, the image of the neutron souce is formed at b=43cm with the combined concave reflecting system. This calculation supports the focusing effect. The result described in(2)(b), on the other hand, suggests a decrease of the primary extinction with the bending.

It is possible to increase the thickness of the assembly up to 1.5 to 2cm, which is expected to increase the intensity to a considerable degree. The focusing effect greatly depends on the geometrical cnfiguration.

Farther tests, including the test to increase the assembly thickness, is being planned.

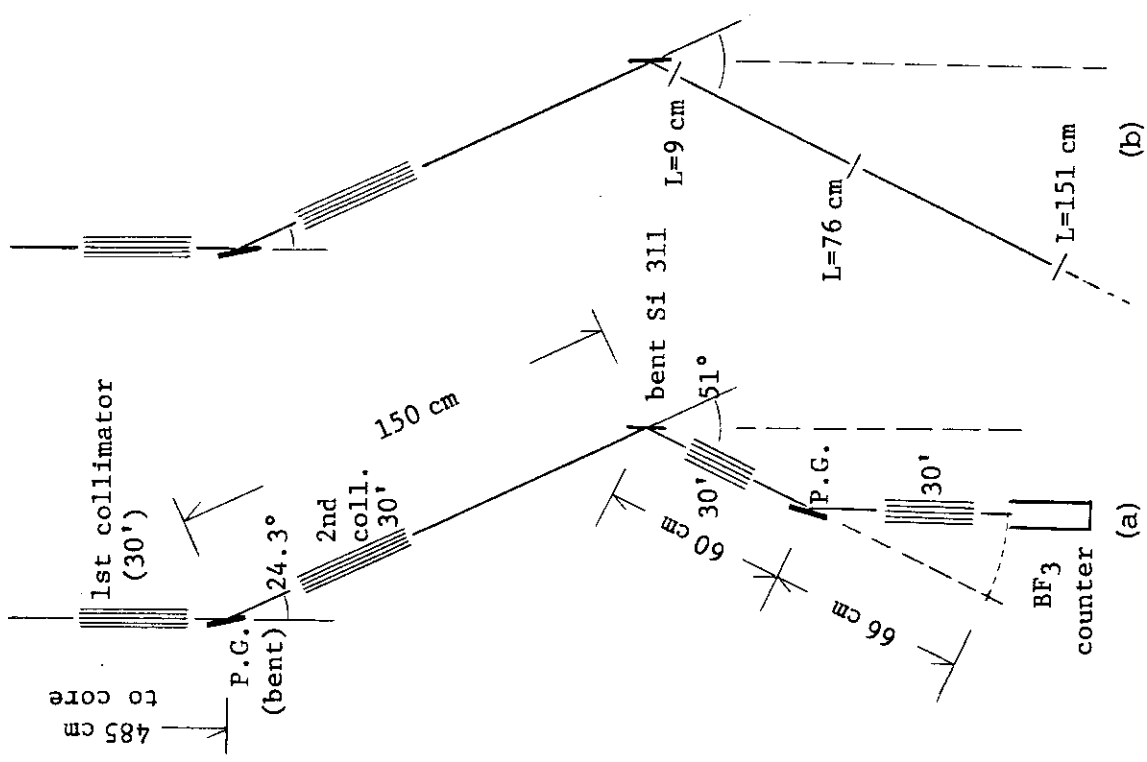

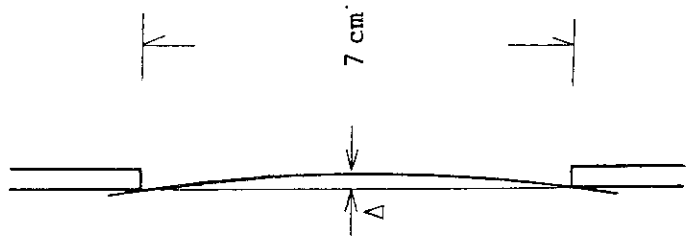

Fig.1
(a) Geometrical configuration used for θ-2θ and rocking curve measurements with various bending.
(b) Positions where photographs were taken. Analyzer and counter were moved away.
(c) Bending of the sliced plates.

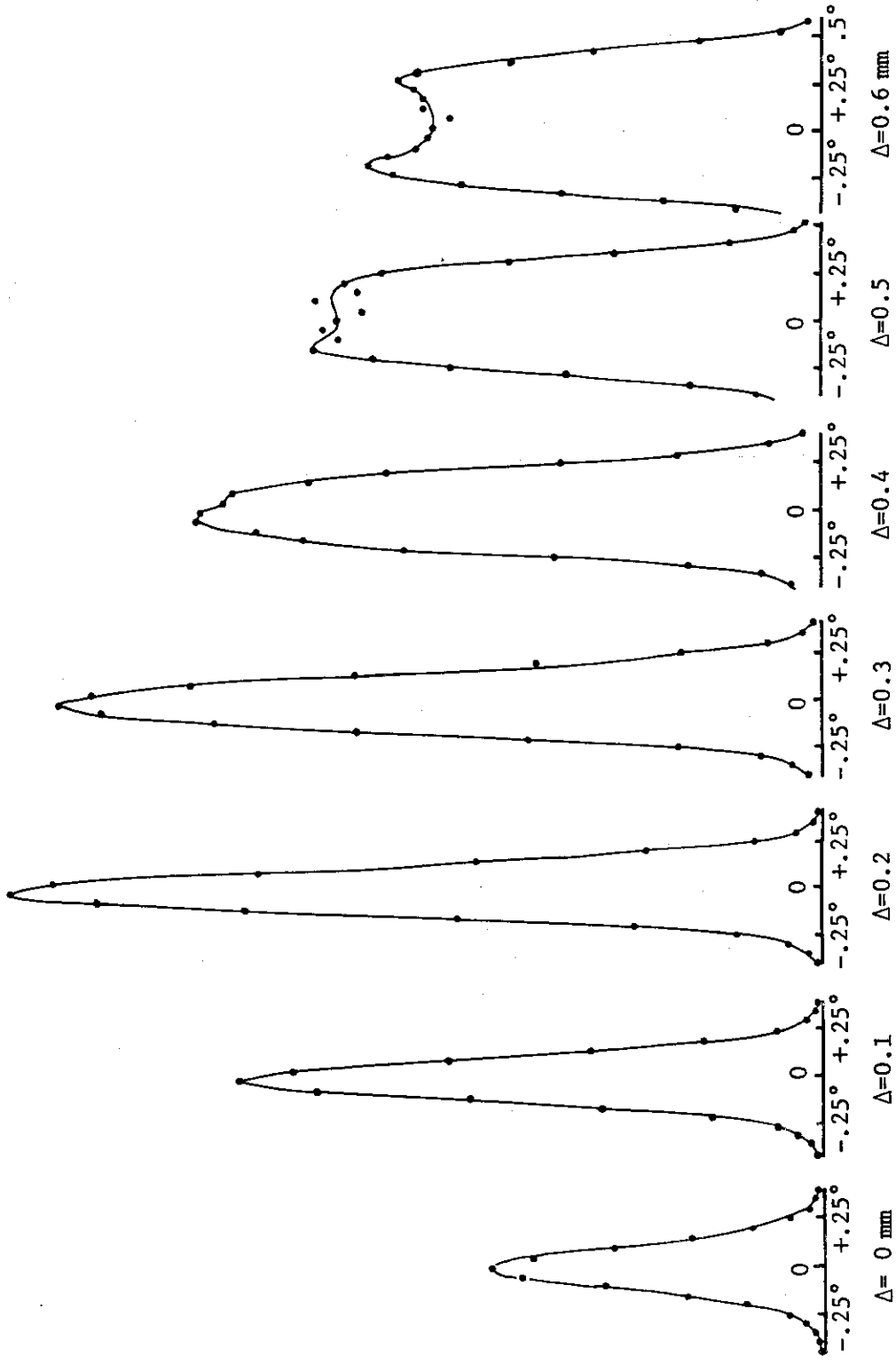

Fig.2 Change of rocking curve of a single 0.5mm thick Si 113 plate with bending.

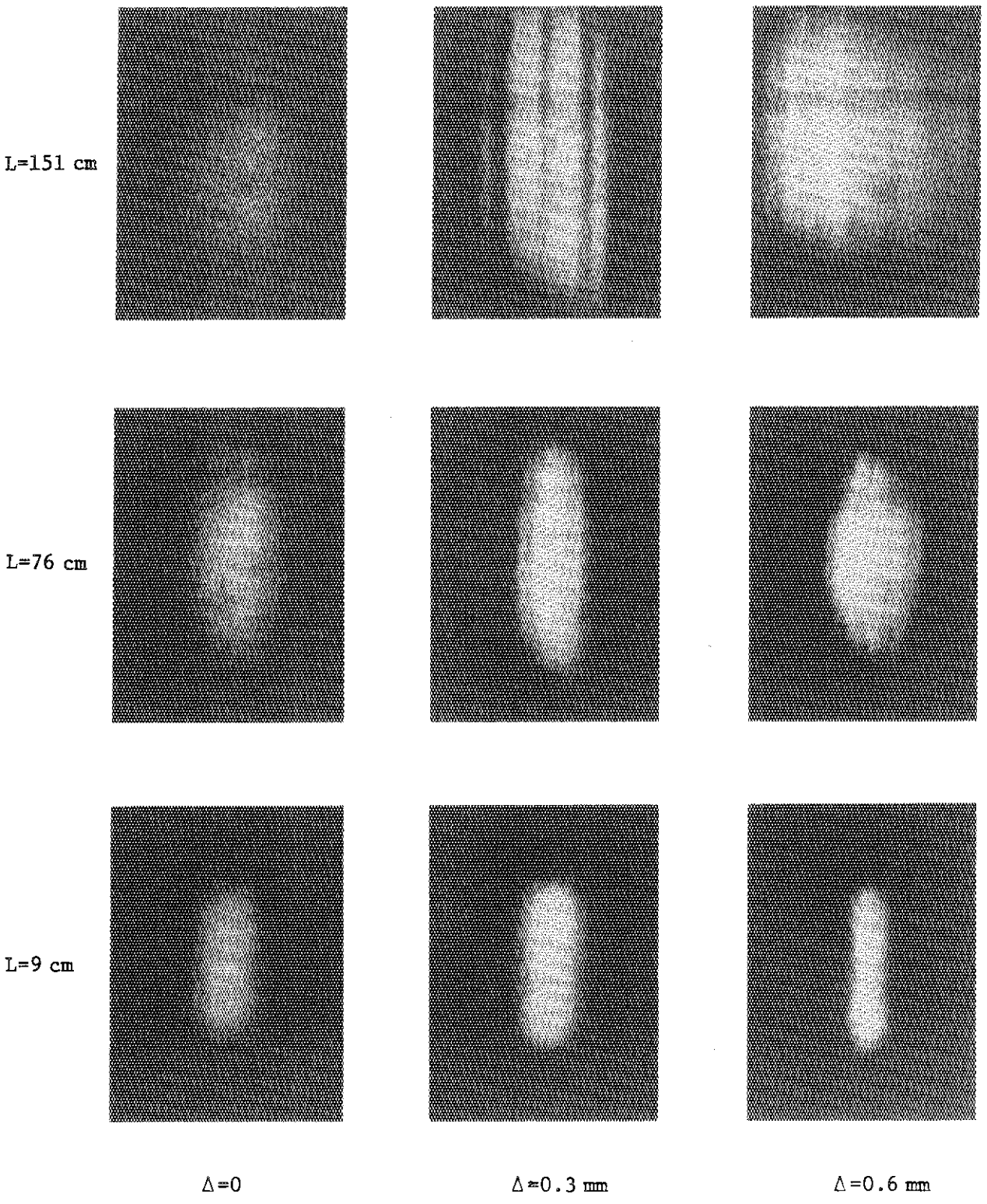

Fig.3 Photographs of neutron beam diffracted with a single 0.5 mm thick Si 113 plate. L is the distance between the Si plate and the neutron camera. Δ is displacement at the center of the plate by bending.

III. RESEARCH

1. KINETICS OF FIRST-ORDER RECONSTRUCTIVE PHASE TRANSITIONS

M. Iizumi, S. Katano, H. R. Child and R. M. Nicklow

When a thermodynamic variable (say temperature, in the present case) of a system is changed abruptly beyond a phase boundary of an equilibrium phase diagram the system is brought to a metastable state, if the first order phase transition takes place at the boundary. Then the system starts to change toward the equilibrium state. The kinetics of this process is an old problem of the rate and kinetics theory of phase transitions. The interest in this old problem revived recently with the growing interests in the statistical mechanics of non-equilibrium states.

One of the research area proposed from the early stage of the conceptual design of the wide-angle neutron diffractometer was to use its fast data-acquisition capability to study the kinetics, i.e. time-dependent change of the crystal- or micro-structure of a system brought into a metastable state.

As a first series of measurements in this direction the kinetics of the reconstructive structural phase transitions was studied. The reconstructive phase transition is a kind of structural phase transitions where the primary coordination (first-nearest neighbor) bonds are broken and reformed. The structures before and after the phase transition are so different that the only way the transformation can occur is by disintegrating one structure and reconstruct the other. There is a sharp contrast between this type and the displacive or martensitic structural phase transitions where the primary coordination bonds are maintained and the transition takes place by collective displacements of constituent atoms.

There is no symmetry relation between the two phases separated by a reconstructive transition. Since the reconstructive phase transitions give rise to large discontinuities in cell dimensions, symmetry, internal energies and other physical properties, the energy barrier involved in this type of phase transitions is generally high. Therefore the transitions may proceed according to the nucleation and growth mechanism. The transition starts from fairly drastic atomic rearrangements within very small localized volumes, called nuclei, formed accidentally in the original phase by a large thermal fluctuation which brings the size of the

volumes beyond a certain critical size. And then the nuclei grow at the expense of the original phase by the relatively slow migration of the interphase boundary resulting from atom by atom transfers across this boundary.

We carried out two measurements: a phase transition from NaCl-like to CsCl-like structures in $RbNO_3$ and a transition between alpha and beta phases in tin(Sn).

I. $RbNO_3$

Rubidium nitrate ($RbNO_3$) shows a series of three phase transitions among CsCl-like structures(IV and III) at low temperatures and NaCl-like structures (II and I) at high temperatures. We studied only the transition from the phase III to the phase II, since the phase transition shows the largest hysteresis and the most conspicuous changes in diffraction patterns among the three transitions.

After a rapid temperature-change from a temperature below Tc (transition temperature T_c = 500 K) to $T_c + \Delta T$, the diffraction patterns were recorded by using the time-slicing mode of the instrument. The observed patterns are overlap of the one diffracted from the phase III part of the sample and the one from the phase II part growing within the sample. The fraction of phases III and II in the sample was derived from the mixed diffraction pattern of each time slice by fitting Gaussian line shapes to typical diffraction peaks corresponding to each phase.

In principle we could have obtained information on the size of the growing phase-II particles (or domains) from the widths of the Gaussian line shapes. But it was not possible to obtain reliable set of size data both because at the initial stage of the change the phase II peaks were too weak for a good fitting to be carried out or because at the later stage the particle size is too large compared with the upper limit of the size we could determine with the present instrumental resolution.

Full courses of the fraction change were observed for several values of ΔT, ranging from 1 to 26°C. For a large temperature jump (i.e., a high degree of metastability), the change took place very fast and finished within 10 minutes while for a small jump (i.e., a low degree of metastability), the change was so slow that it took more than 60 minutes to finish. The experimental possibility of measuring a rapid process was

found to be limited in practice by how rapidly the temperature of the furnace can be changed and by how fast the temperature of each part of the powder sample follows the change.

The volume fraction transformed at time t is known to be expressed generally by the so-called Avrami or Johnson-Mehl equation (hereafter this equation will be abbreviated as AJM equation).

$$x(t) = 1 - \exp[-(t/\tau_0)^n] \qquad (1)$$

where the relaxation time τ_0 depends both on the nucleation rate and the growth speed. The exponent n = 4 was originally proposed by Avrami for the case where the nuclei are formed homogeneously and the nucleation rate is constant in time and further the growth takes place isotropically with a constant velocity. Actual experimental situations are different from the ideal case assumed by Avrami. It is, however, known that most of the situations can be covered by the choice of exponent values different from 4. For example if the nucleation sites are limited in number and the nuclei are formed at the start and there is zero nucleation after that we obtain n = 3 for the linear isotropic growth and so on. It is therefore convenient to make the exponent as well as the relaxation time as fitting parameters to the experimentally observed x vs. t relations and see what sort of values we obtain as the results of least-square fitting. The x vs. t curves for several selected values of n are illustrated in Fig. 1.

Details of the results of analysis on $RbNO_3$ are not given here. They indicate that the values of the exponent are about one irrespective of T. This implies that the kinetics follows the first-order rate process in which the probability of any small region transforming in a given time interval is the same in all parts of the untransformed volume, that is to say no nucleation is necessary and the transformation proceeds homogeneously and spontaneously in this case. This conclusion, however, are not so convincing since the analysis is seriously affected by the lack of data for the early stage of the evolution in time. The observation of a finite incubation period, during which no new phase is apparently formed, is essential for the departure of the kinetics from the homogeneous transformation. The observation of early stage was limited because of the limited speed of the temperature change within the sample in this case. The relax-

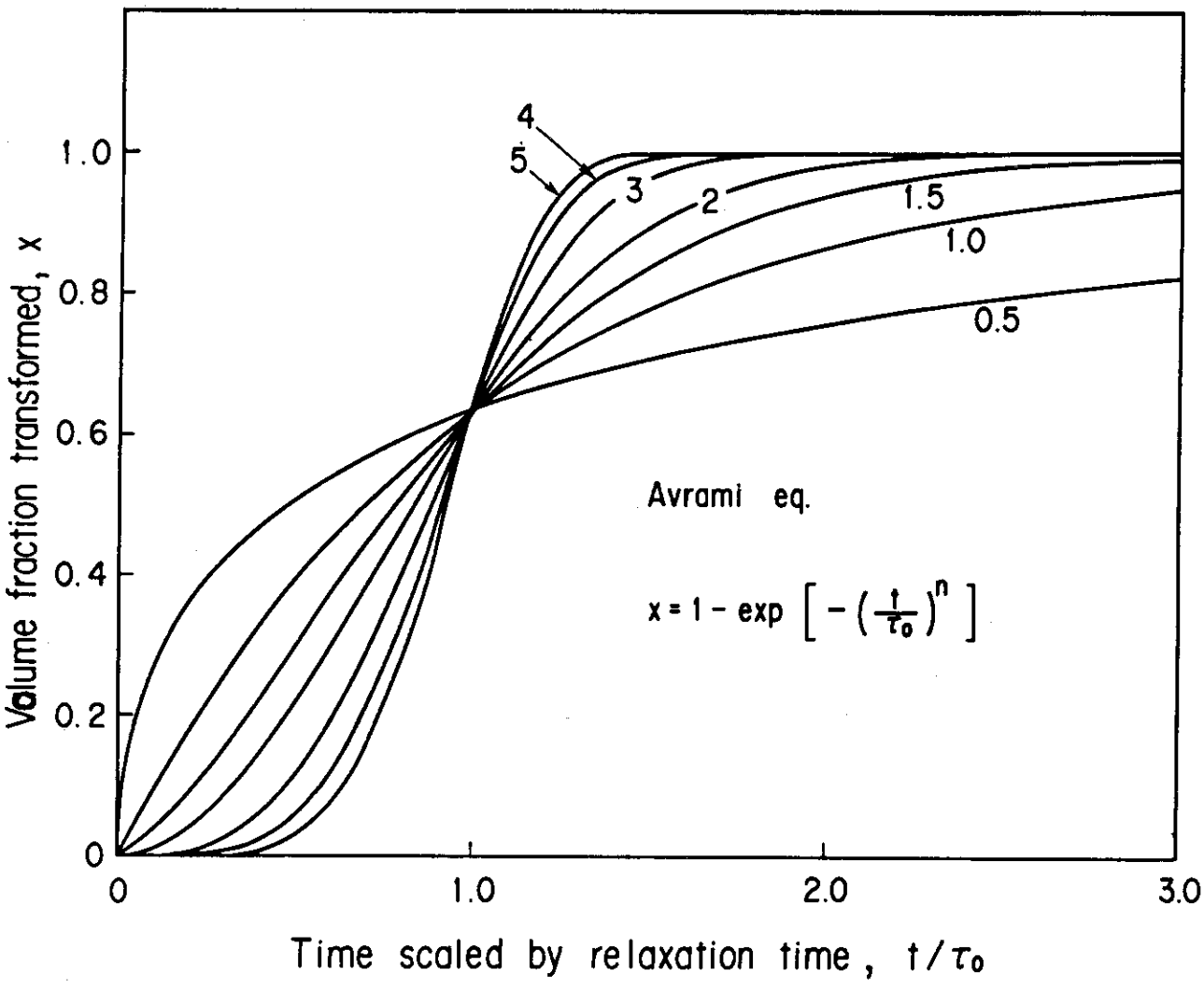

Fig. 1. Change of the volume fraction transformed at time t according to the Avrami-Johnson-Mehl equation (1) for several choice of the exponent n.

ation times indicate the critical slowing down in approaching the transition temperature.

II. Sn

At room temperature tin (Sn) is metallic and called white tin, or beta phase tin. The white tin transforms to gray tin, or alpha phase tin below about 260 K. The gray tin is semiconducting and has a diamond structure like germanium or silicon, while the white tin has a special tetragonal structure found only in this element.

The beta-to-alpha transition is fairly slow, taking from 1 to 12 hours, depending on temperature. The reverse transition from the alpha to the beta phase occurs above about 290 K and the change becomes very rapid as the temperature increases. Extensive measurements were carried out on both the alpha-to-beta and beta-to-alpha transitions.

Fine-powder samples of alpha or beta phase were prepared from white tin grains (99.999% purchased from Mitsubishi Metal Co.) by repeated temperature cycles between 230 K and 330 K. The first transition to alpha phase in the grained sample was found to be very hard to initiate. The transition started rather accidentally at a spot on the surface of some limited number of grains and proceed very slowly. The contact with a transformed region generates nuclei of the new phase on another grain. The initial transition proceeded in this way. First we planned to use the 99.9999% white tin sample purchased from another company but it was found hard to transform this sample to the gray tin. So we used the Mitsubishi sample. Later it was found the another sample can be transformed by mixing the sample with the gray tin powder obtained from the Mitsubishi sample.

The Displex system was used to change the sample temperature on the diffractometer. In case of the beta-to-alpha transition the sample was kept at 320 K for at least 30 minutes and then the temperature was started to cool down toward a target temperature. Because of the limited cooling power the temperature drop is rather slow (about 10 K / 5 min). So there is an ambiguity about the origin of time-change. We took the time when the temperature crossed 263 K as the origin. This is the boundary temperature where the beta-to-alpha transition does not actually take place. Since the kinetics is rather slow in the case of the beta-to-alpha transition the ambiguity of the time origin does not matter at all.

In the case of the alpha-to-beta transition the sample is kept at 230 K for at least two hours and the sample was heated up by a heater built in the cold head of the Displex system. The time origin was set at the time when the temperature crossed 290 K for rather slow alpha-to-beta transition. In order to observe the faster change at higher target temperature the time origin is taken as close as possible to the time when the sample temperature reach the target temperature in so far as the time elapsed before the origin is insignificant to observe the kinetics at the target temperature.

The time increment in the time-slicing measurement was chosen within the range of 1 to 30 minutes in accordance with the speed of the kinetics. Unequal time slices was convenient to record the whole course of change in 16 time slices (In principle the system was designed in such a way that up to the 48 time slices are available. But during the present measurements we were using twice as large time channels for a single time slice and also one histogramming memory unit was in disorder).

A typical change of the diffraction patterns during the transient is illustrated in Fig. 2 which shows a limited part of the whole diffraction patterns for only a few selected time slices.

A diffraction pattern at time t, f(s,t) is a superposition of that in pure alpha phase, $f_a(s)$, and that in pure beta phase, $f_b(s)$:

$$f(s;t) = p_a(t)f_a(s) + [1-p_a(t)]f_b(s), \qquad (2)$$

where s indicates the scattering angle or the channel in the recorded data and $p_a(t)$ indicates the fraction of existing alpha phase. The diffraction patterns of the pure alpha and beta phase were measured before and after one series of time-slicing measurements and are indicated and compared in Fig. 3. The entire diffraction patterns were used to determine the fractions of existing alpha and beta phases in the respective time slice. This was done simply by fitting the above overlapped pattern with unknown fraction $p_a(t)$ to the observed pattern at time t.

Fig. 4 summarizes the results for the beta-to-alpha transition. In this figure the obtained $p_a(t)$'s are shown as functions of time t for various final temperature. The $p_a(t)$ curves follows typical nucleation-and-growth kinetics; they have fairly long incubation times during which

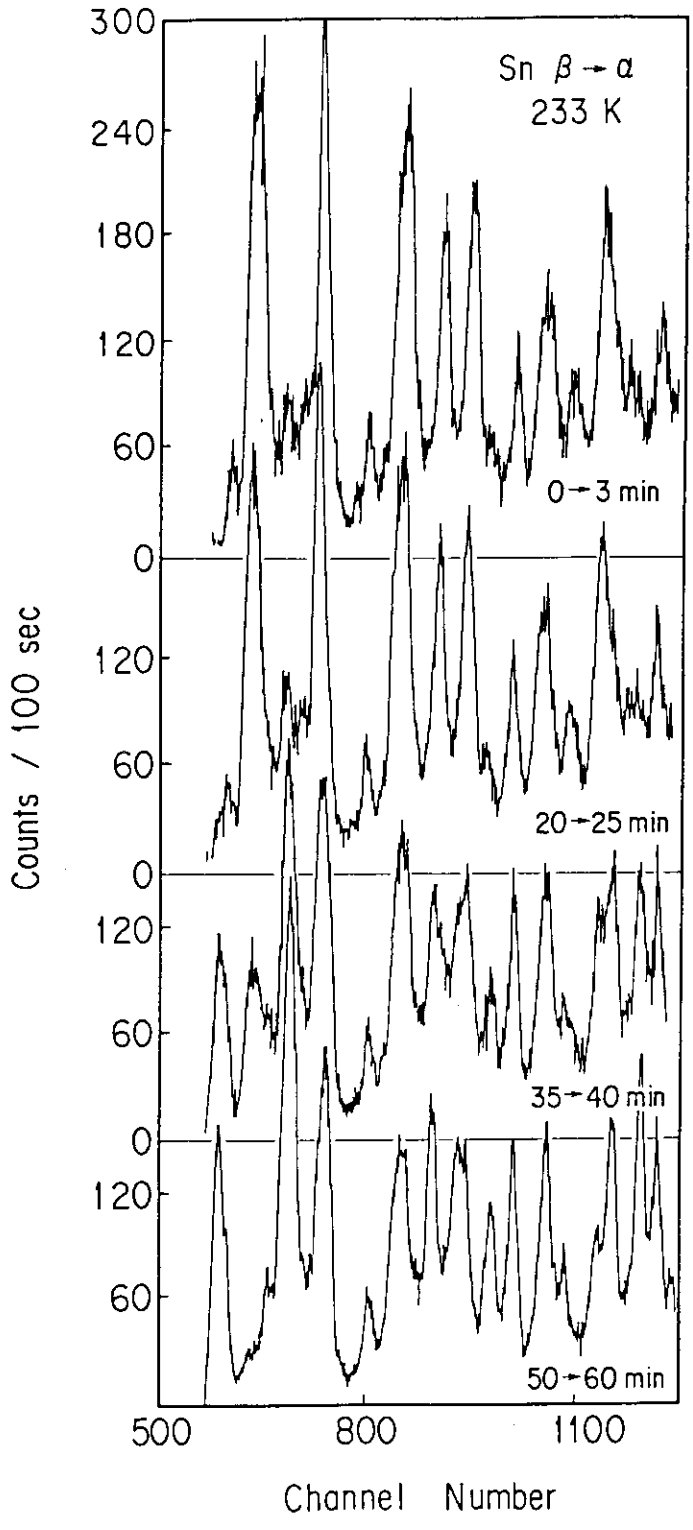

Fig. 2. Change of diffraction patterns with time measured by the time-slicing function of the wide-angle neutron diffractometer. The results shown are for the change after the tin sample are cooled down from the high-temperature beta phase to 233 K where the alpha phase develops.

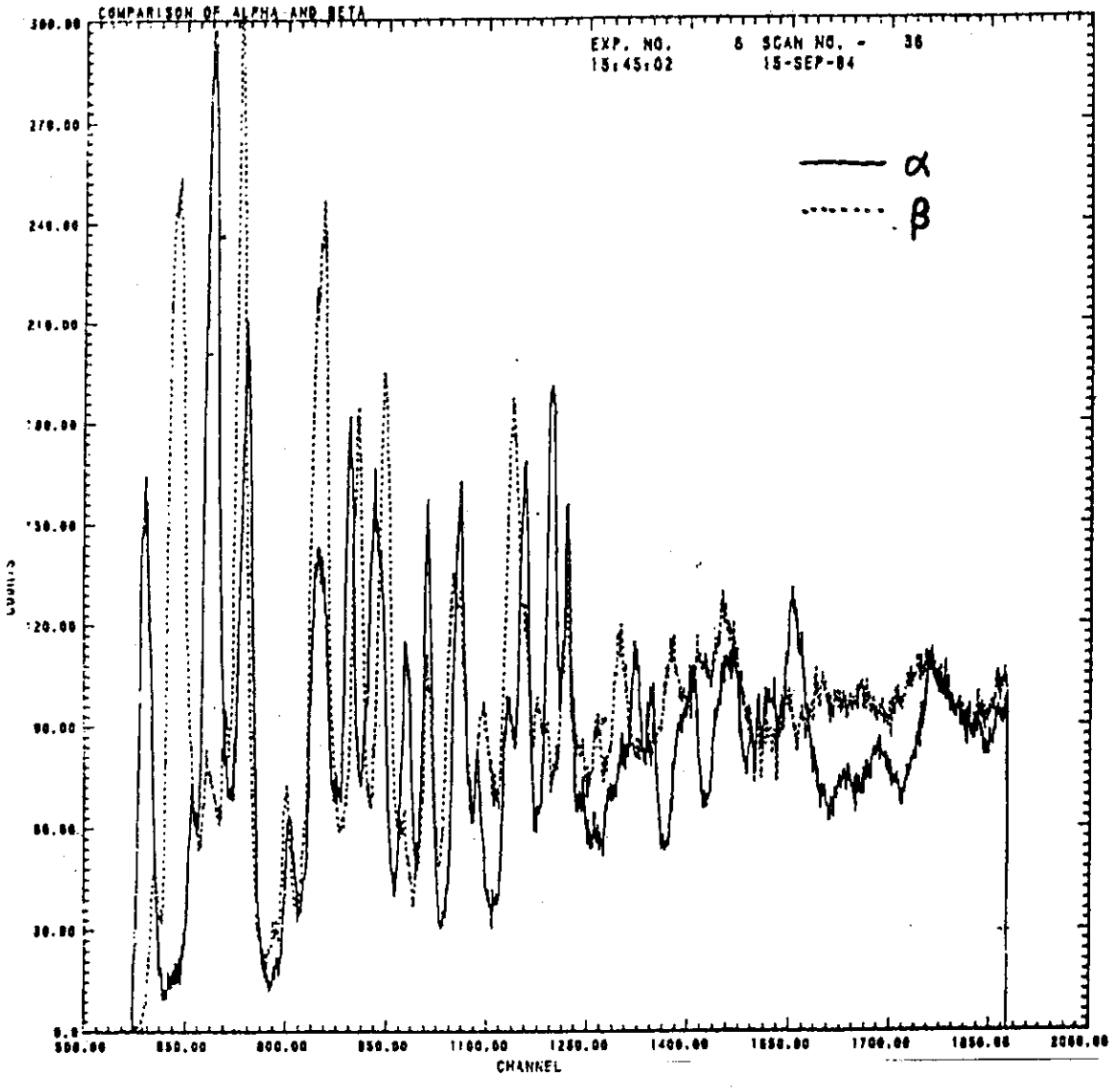

Fig. 3. Comparison of neutron diffraction patterns for the alpha and beta phase of tin measured by the wide-angle neutron diffractometer.

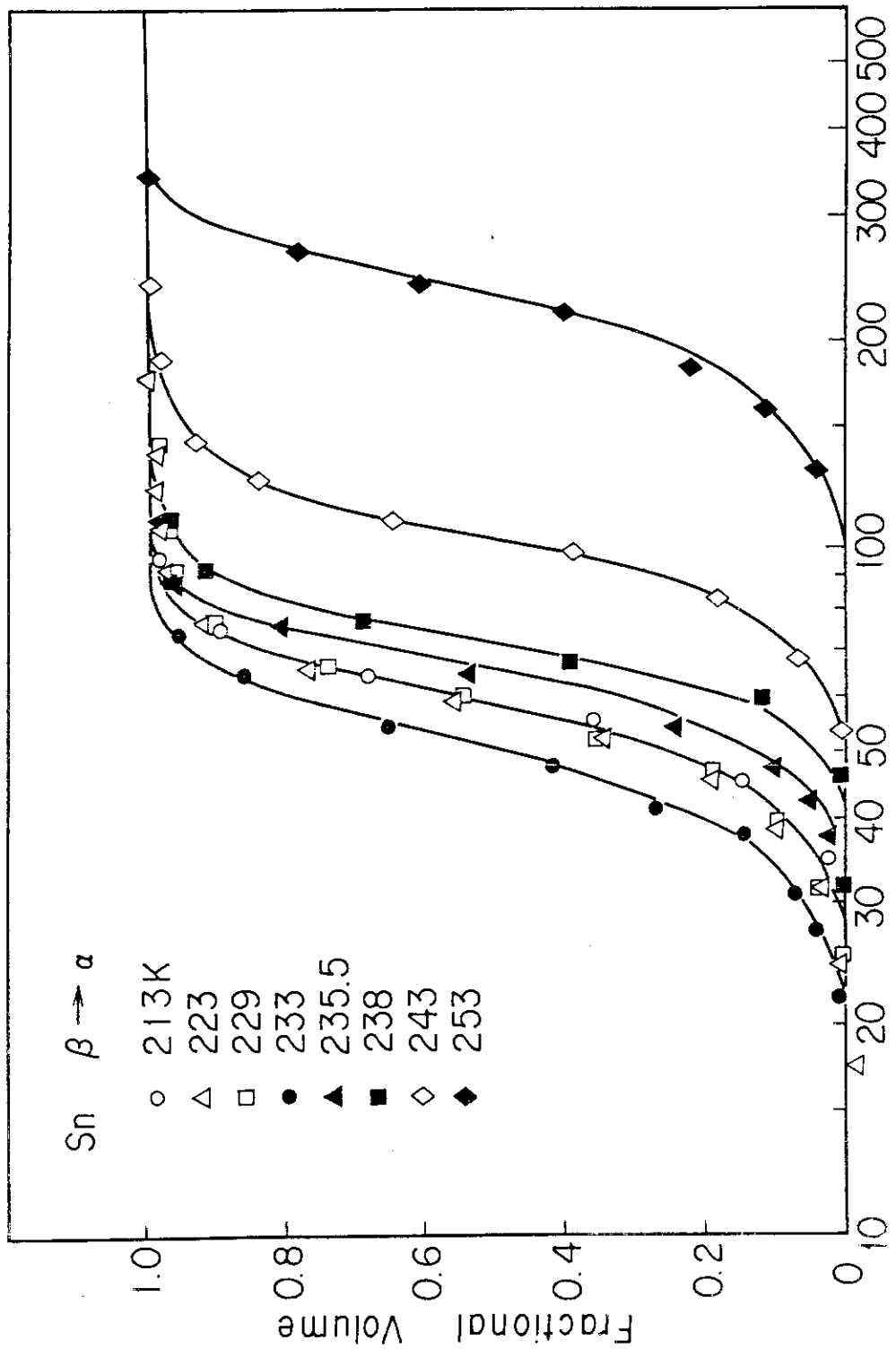

Fig. 4. Measured change of the fractional volume with time for the beta to alpha phase transition for various choice of the final tempertures.

the metastable phase does not show any change and then the new phase starts to appear first gradually and becomes quite rapid and finally becomes sluggish. The change is most rapid at the final temperature around 233 K and becomes slow at temperatures either higher or lower than this value. Similar results were obtained for the alpha-to-beta transitions which are shown in Fig. 5. It seems that there were some experimental problems in the measurements for the final temperature of 300.5 K and 305.5 K.

The time dependence of the transformed fraction was then fitted to the JMA type equation given in Eq.(1) with the relaxation time and kinetics exponent as fitting parameters. The results are summarized in Fig. 6 where both the alpha-to-beta and reverse transitions are indicated. The relaxation time shows the slowing-down behavior as temperature approaches the transition temperature from both sides. The characteristic exponent of the kinetics is about 5 in the alpha-to-beta transition and about 2 for the beta-to-alpha. The typical exponent of the JMA equation is 4 when the nucleation rate is constant and the growth rate is linear. With linear growth rate the exponent larger than 4 means that the nucleation rate increases with time, that is it takes a long time to attain the equilibrium distribution of nuclei. This seems to be the case in the alpha-to-beta transition. The exponent below three can not be explained by the isotropic growth. The exponent 2 just correspond to the case of two-dimensional growth from the nuclei generated instantaneously at grain edges.

The JMA type equation automatically satisfies the scaling with respect to time, that is, if the time is scaled by the relaxation time ($\tau = t/\tau_0$) then the kinetics follows the universal equation

$$x(\tau) = 1 - \exp(-\tau^n) \qquad (3)$$

irrespective of the final temperature. This means that in approaching to the equilibrium from the metastable state the system follows the same mechanism at any temperature and that the speed of whole evolution process is controlled only by a single time scale which is the relaxation time. This property was confirmed by plotting the $x(\tau)$ obtained for the respective final temperature on the same figure as shown in Fig. 7 (beta-

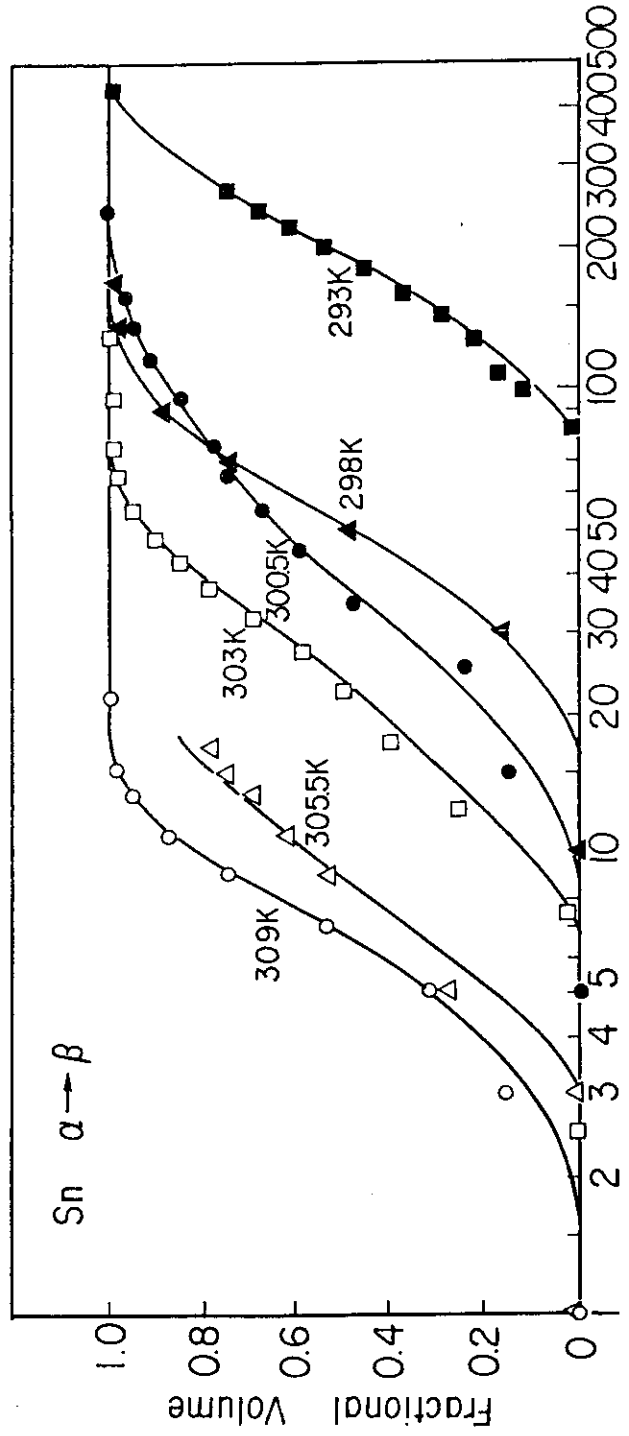

Fig. 5. Measured change of the fractional volume with time for the alpha to beta phase transition for various choice of the final temperatures.

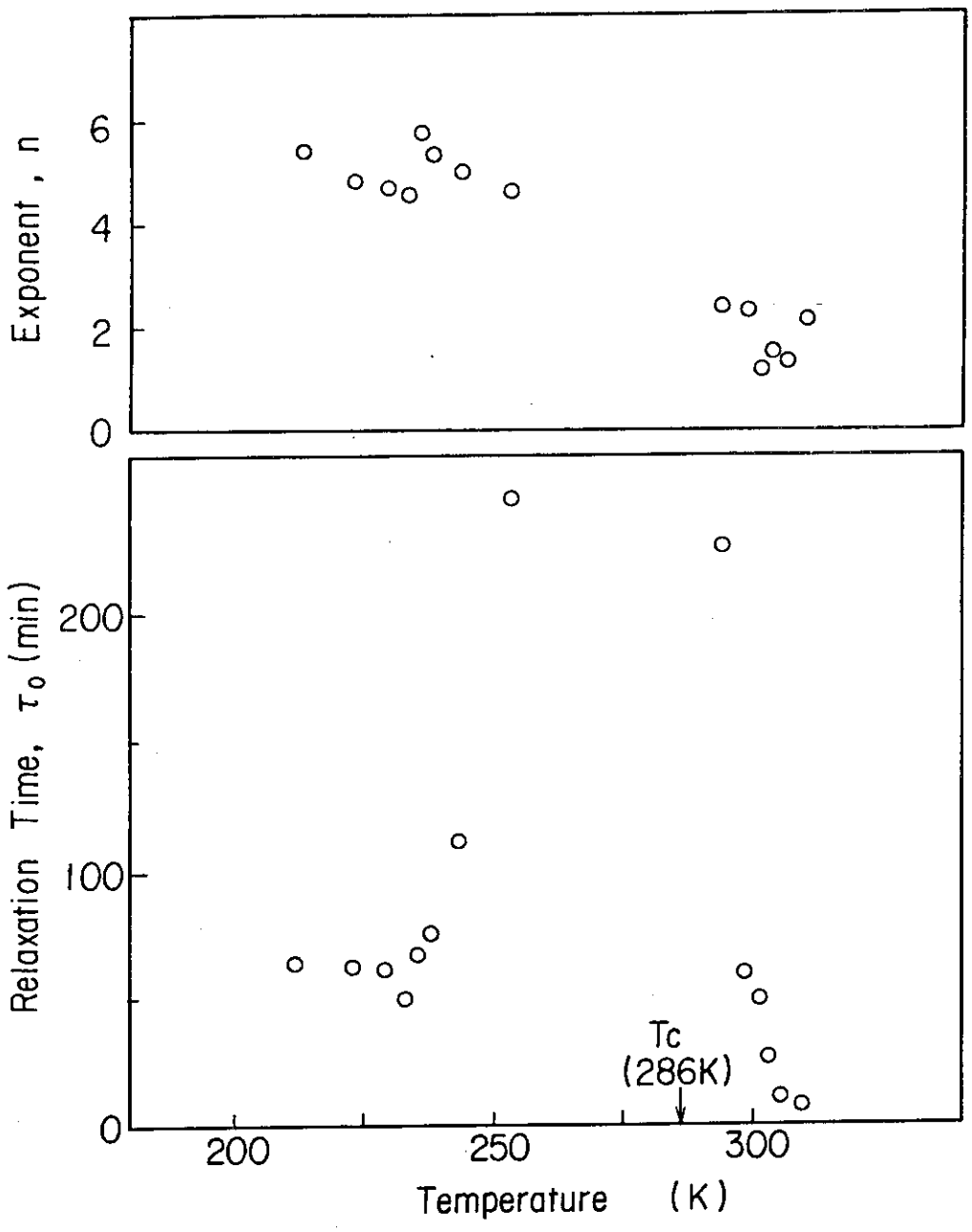

Fig. 6. The relaxation times and exponents obtained as results of the fitting are shown as functions of the final temperatures.

to-alpha) and 8 (alpha-to-beta) where use was made of the relaxation time obtained by the fitting for each data set to scale the time. In the case of beta-to-alpha transition the scaling property applies almost perfectly with n = 5, while in the case of alpha-to-beta transition there is some discrepancy with the exponent n scattering from 1.3 to 2.3, which might come from the experimental irregularity.

In this case we also tried to unravel the information concerning the size of the transformed region at the early stage of the transition. The plot of, say

$$f(s;t) - [1 - p_a(t)]f_b(s) \qquad (4)$$

shows the contribution only due to the alpha region. The plots at the early stage of the beta-to-alpha transition were investigated to find diffraction peaks wider than those in the pure alpha phase diffraction pattern. We noticed some sign of the widened peaks but the poor statistics and the large instrumental width prevented us to obtain reliable information with respect to the particle size.

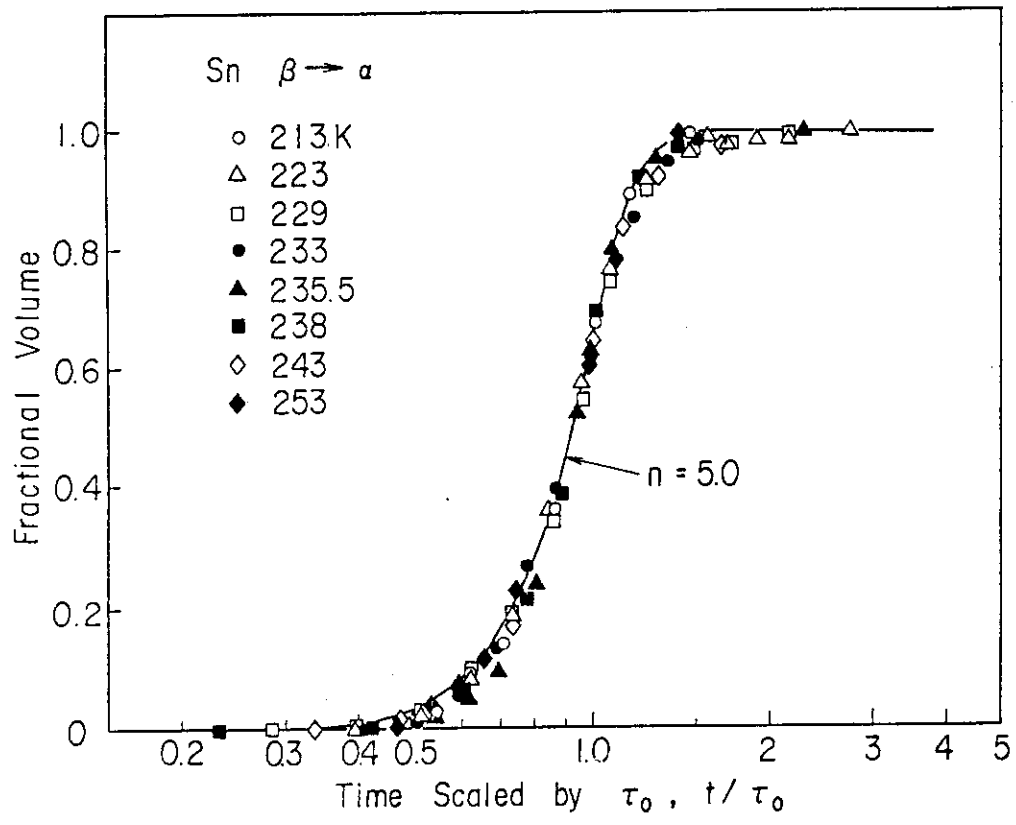

Fig. 7. Scaling behavior of the fractional volume with respect to time measured for the beta-to-alpha transition in tin

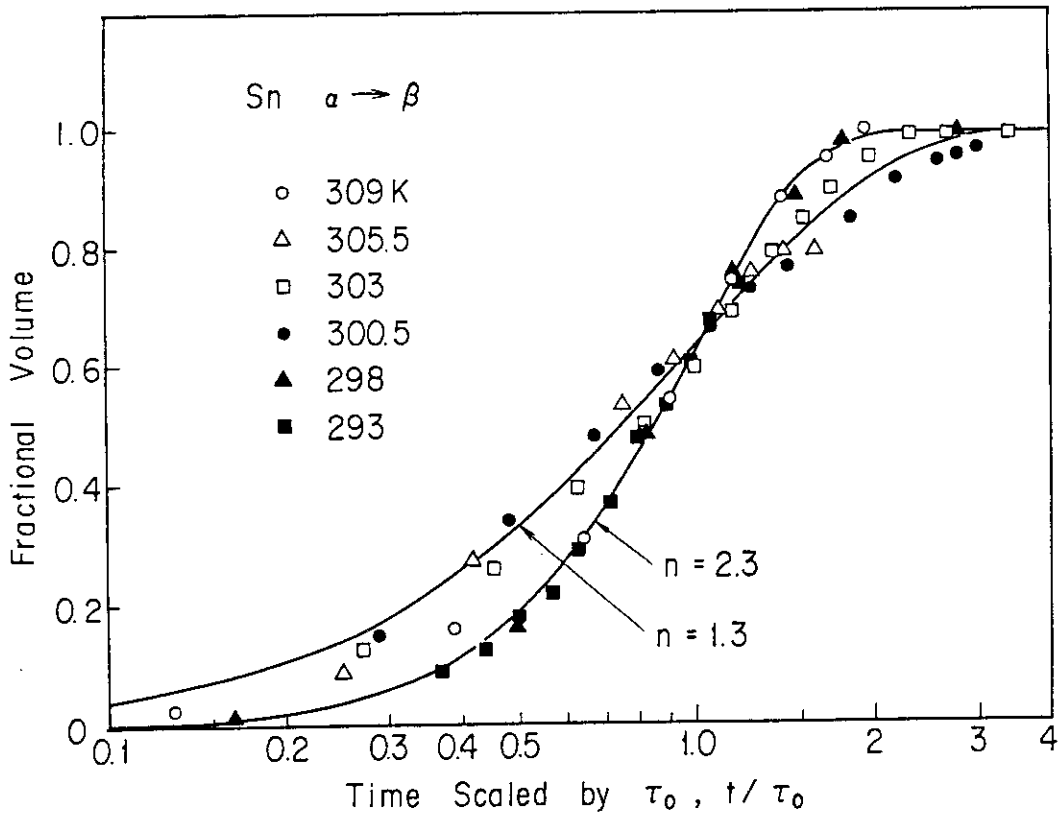

Fig. 8. Scaling behavior of the fractional volume with respect to time measured for the alpha-to-beta transition in tin.

2. POWDER NEUTRON DIFFRACTION OF MAGNETIC MATERIALS

S.Funahashi, S.Katano, O.A.Pringle and H.R.Child

Some diffraction experiments of magnetic materials were carried out by using WAND in November 1984. The samples measured were $Lu_2Fe_3O_7$, Cr-Re alloys and κ-MnGe alloy.

(1) $Lu_2Fe_3O_7$; This material has a hexagonal layered structure. Two kind of iron layers named V-layer and W-layer which are composed of Fe_2O_3 and Fe_4O_5, respectively, are separated with nonmagnetic layers composed of Lu_2O_3[1]. It is presumed from Mössbauer experiment [2] that two-dimensional magnetic order begins to develop in W-layer at 260K while the V-layer remains paramagnetic down to 80K, below which two-dimensional magnetic order grows in this layer, too. No significant difference between the neutron diffraction results at about 100K and 40K was observed in the previous experiment[2]. In order to investigate this problem, a detailed temperature dependence was measured.

Since lutetium absorbs thermal neutrons considerably ($\sigma_a=76\times10^{-24}cm^2$), a sintered sample of cylindrical shape of 3mm diameter was used. Fig.1 shows the diffraction patterns at various temperatures from which the room temperaure diffraction has been subtracted. The measuring time was several hours for each one. Broad asymmetric diffractions which are typical for the low-dimensional diffraction are seen. The diffraction arises from a 1/3 1/3 ζ line in the reciprocal space. Fig.2 shows the temperature dependence of the integrated intensity for $2\theta=15\sim22.5°$. The data points are too scattered to draw any conclusion from this result. The statistical error is smaller than 0.1 percent. The large scattering of the data points is presumably due to changes of the back ground during the measurements.

Another question of this material is whether there is any preferred orientation along the cylinder axis in the sintered sample made from pressed materials. A cylindrical sample of 3mm diameter × 3mm length was measured setting the cylinder axis in the scattering plane. Fig.3 shows the diffraction patterns measured at every 6 degrees of turning angle of the cylinder axis in the plane. The measuring time was about 40 minutes

for each one. The result shows that there is no significant preferred orientation in this sample. WAND is obviously very effective to carry out this kind of experiment. It is practically impossible to do this kind of measurement with the conventional diffractometer within reasonable measuring time.

(2) Cr-Re alloys; This system becomes antiferromagnetic at low Re concentration while it becomes superconductive at higher Re concentration. The critical region is about 18 percent Re. Neutron diffraction was measured of 18 percent and 20 percent Re samples. The incident neutron wavelngth was 1.75Å as Be 100 reflection was used to monochromatize the beam. Fig.4 shows the result at room temperature. Most of the peaks, except for the four strongest peaks, are the diffractions by the half wavelength component included in the incident beam from Be 200. Though slight changes of the diffraction intensity were observed for most of the peaks at low temperature, the changes were too small to discuss magnetic structure considering the large half wavelength component. The weak 100 diffraction should be absent in bcc crystals. It was observed afterward in JAERI carefully eliminating the half wavelength component that a very weak, presumably magnetic, 100 reflection which changes with temperature exists.

(3) κ-Mn_5Ge_2; This material is a ferrimagnet having a compensation point of sublattice magnetization at 400K and the Curie temperature is 710K. The orthorhombic unit cell consists of 28 atoms. Fig.5 shows a diffration pattern measured at room temperature. The strongest diffraction is 211. The intensity of the two peaks at lower angles does not seem to change with temperature while many diffractions at higher angles including 211 change at lower temperature. The structure is, however, considerably complicated to be analyzed from the present results. Improvement of the position resolution and the elimination of the half wavelength component are needed.

Summary

In magnetic neutron diffractions, strong scattering occurs at low Q region due to magnetic form factor. On the other side, the lowest scattering angle reached with the WAND machine is limited mechanically. It is, therefore, preferable to use rather long wavelength neutrons. The long wavelength neutron has another merit to resolve close peaks. The present wavelength of 1.75Å is suitable for magnetic diffractions from this view

point. Though the present experiments gave fruitful output only for the test of the preferred orientaion, the results indicate that some improvements -- (1)elimination of the half wavelength component in the incident beam, (2)higher position resolution, (3)lower background -- will make WAND a very powerful machine for magnetic diffraction.

References

[1] K.Kato et al., Z.Krist. 143(1976)278.

[2] M.Tanaka et al., J.Magn.Magn.Mat. 31-34(1983)769.

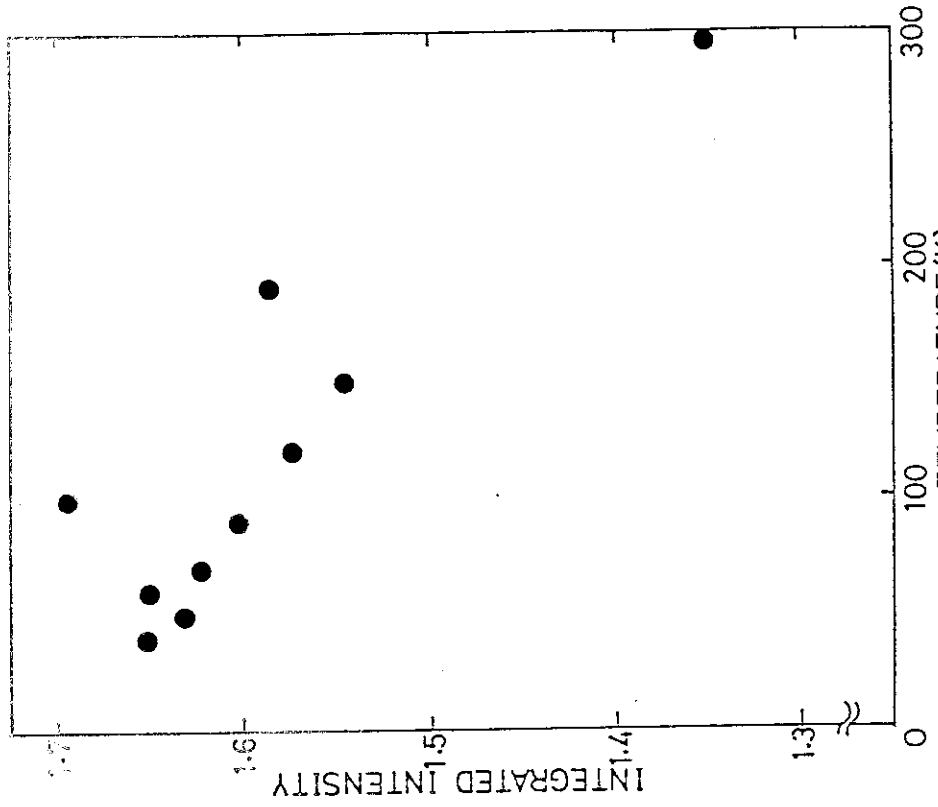

Fig.2 Temperature dependence of the integrated intensity for 2θ over 15~22.5°.

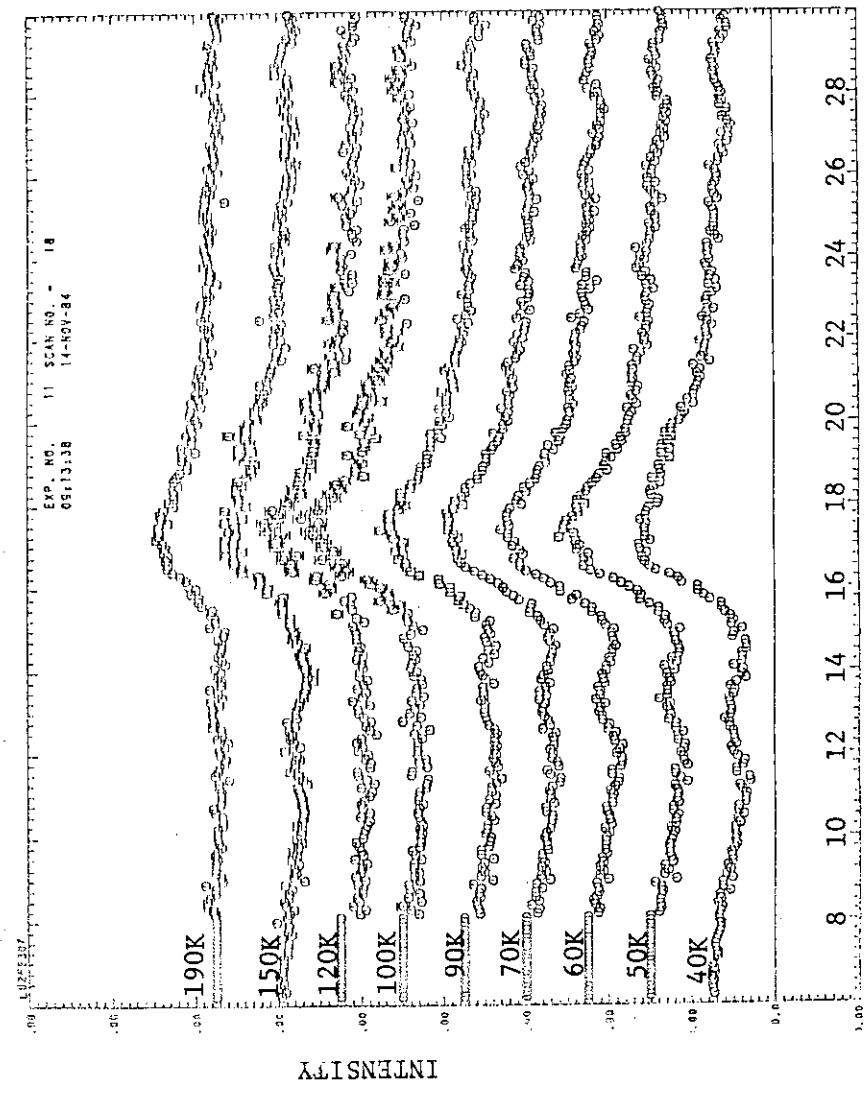

Fig.1 Temperature dependence of diffraction pattern of $Lu_2Fe_3O_7$. Figure shows the remainder after the subtraction of the room temperature pattern.

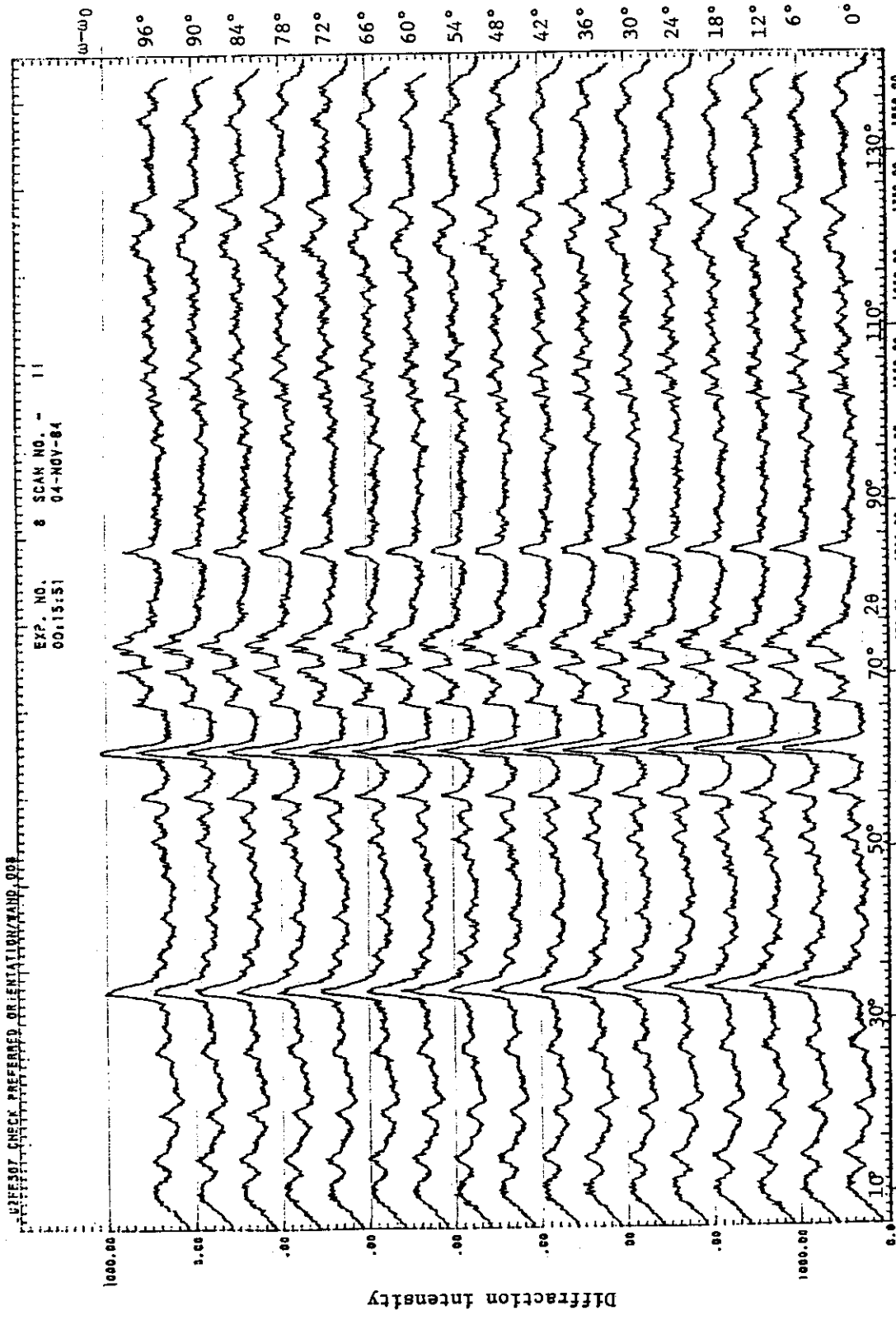

Fig.3 Diffraction patterns of pressed and sintered $Lu_2Fe_3O_7$ measured at every 6 degrees of different orientation of the pellet axis. No significant preferred orientation is observed.

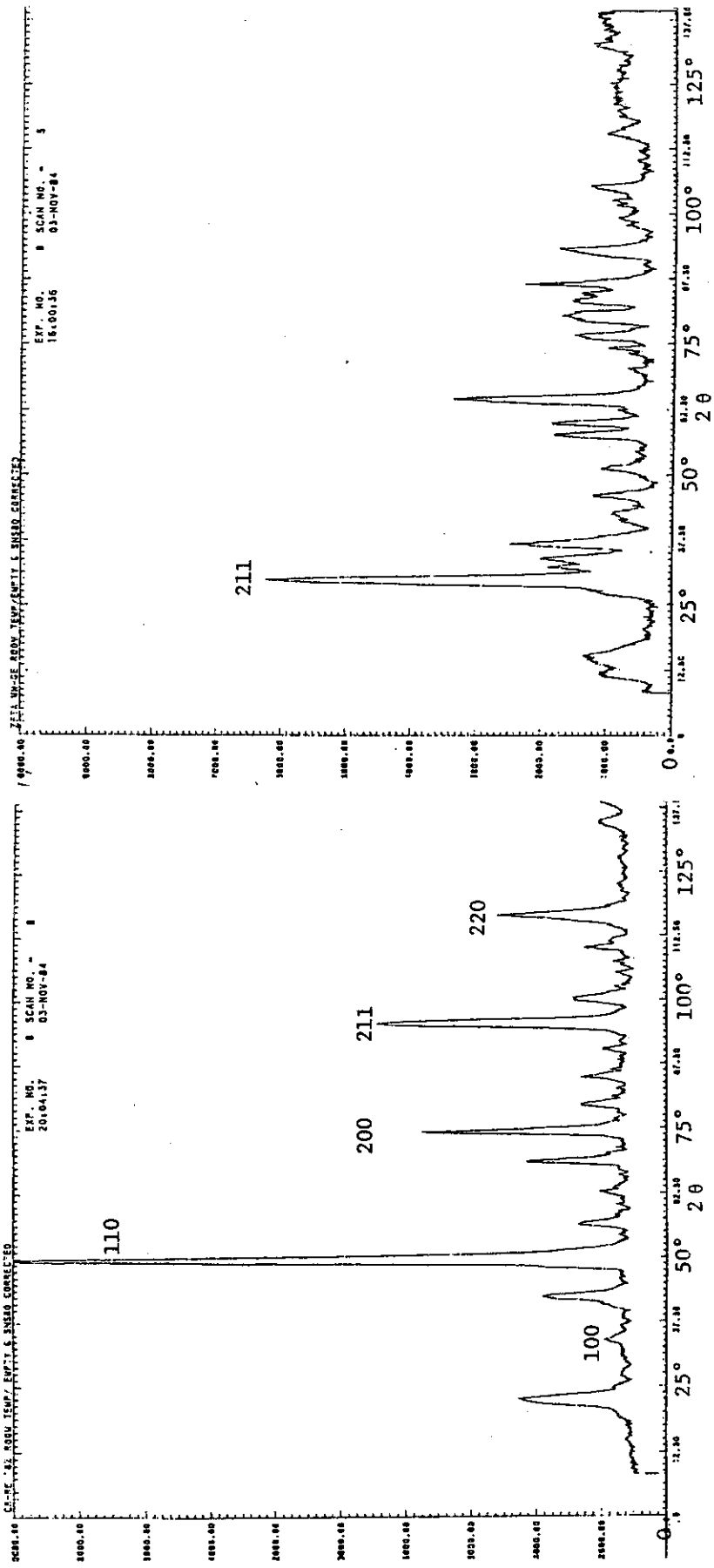

Fig.4 Diffraction pattern of Cr-Re(18%) measured at room temperature. Most of the unindexed peaks are λ/2 diffractions. The lowest angle peak (2θ=20°) is 1/2 1/2 0, for example.

Fig.5 Diffraction pattern of κ-Mn_5Ge_2 at room temperature.

3. ORDERING KINETICS IN NI_3MN

S. Katano, M. Iizumi, H. R. Child and R. M. Nicklow

Recently the kinetics of a first-order phase transition has received great attention from both theoretical and experimental points of view. In these time-dependent phenomena, order-disorder transition is one of the most fundamental problems. Hence, many theoretical studies and computer simulations have been done for this subject. As a result, it has been appreciated that in the late stage of the transition the growth of ordered-region follows a power-law of time and the structure factor of a superlattice peak indicates scaling behavior with respect to space and time.

To study this configulational ordering process, Ni_3Mn alloy is an ideal system for the following reasons. (1) Since Ni and Mn atoms have similar size, the elastic strain generated by phase transition should be small. (2) The time constant involved is fairly long. Therefore, neutron diffraction study on the relaxation process of this alloy was investigated by Collins and Teh[1] and that on the ordering kinetics was done by Wakabayashi.[2] However, as they used a conventional neutron diffractometer and furnace, it took over 30 minutes after a change of temperature until the first diffraction pattern was obtained. Hence, it was impossible to observe the early stage of the process and, moreover, we may not be able to disregard a change of the state during the temperature-change and the measurement. In contrast to them, the system of the wide-angle neutron diffractometer and the furnace for rapid change of temperature which are installed in HFIR is the most suitable for clarifying the behavior in the very early stage. Thus, we utilized this system to investigate the whole process from the initial to final stage of order-disorder phase transition in Ni_3Mn.

Figure 1 shows the time dependence of the (211) superlattice peak after temperature is abruptly changed from 600°C to 470°C across the transition temperature around 510°C. The temperature of the sample reached to the final temperature in about 15 seconds. In order to get the result of the initial stage, time-resolved measurement for 1 minutes was done until 30 minutes passed. To increase counting statistics, this measurement was repeated 30 times and each of data for 1 minutes was accumulated. For the final stage, time-resolved measurement for 6 minutes was repeated 5 times. As shown in

this figure, it is observed that the peak becomes sharp with time. This shows the development of order. The width of this peak is shown as a function of time in Fig. 2. It is found that the time-dependence of the width follows power-law and, moreover, the exponent of this law clearly shows crossovers. First, the width remains almost constant, but after time τ_0 it comes to follow the power-law of the exponent of about 1/4, and then after τ_1 the exponent changes to 1/2. These results can be reasonably explained by recent theories[3,4]: The exponent of 1/2 in the late stage has been proposed by several authors in consideration of the motion of the interfaces. This prediction was ascertained by experiments of Cu_3Au by Hashimoto et al.[5] and Noda et al.[6] and of Ni_3Mn by Wakabayashi.[2] Our result in the late stage agrees with these results. On the other hand, Furukawa proposed a more extensive theory[7]; he predicted exponents of 1/3 and 1/4 which come from the diffusion-reaction process. Our result suggests that the exponent is 1/4 rather than 1/3. The earlier stage where the width remains almost constant is considered to be the period of the formation of the ordered-region. Thus, the result indicates that as passing of time the ordering process changes from the stage of the formation of the ordered-region to that of the slow growth of it by diffusion-reaction mechanism, and then to that of the fast growth by the motion of the interfaces. Figure 3 shows the time dependence of the integrated intensity of this superlattice peak. This result indicates that the ordered regions are formed in a very early time and then they grow rather slowly. This result should be explained in relation to the time evolution of the width.

Up to the present, several authors have reported that ordering kinetics shows a critical behavior near the transition temperature.[5,6] However, its detailed property is not clear yet. Therefore, we investigated the ordering kinetics by changing of temperature from 600°C to several temperatures in the ordered state. The results show the same behavior as the result at 470°C with respect to the power-law, hence, we could obtain the temperature dependence of the time τ_0, from when the width begins to follow the power-law of 1/4, and the width Γ_0 at that time. The former is shown in Fig. 4(a). It is clearly seen that τ_0 diverges as temperature approaches the transition temperature T_c which was estimated at 509°C from the temperature dependence of the square root of the integrated intensity at the equilibrium state. Figure 4(b) shows T_c-T versus τ_0 in the log-log scale. As shown in this figure, the slope is about -1. This value is interesting, since Collins and Teh obtained a

similar value in their experiment of the relaxation process in the ordered state.[1] In Fig. 5(a) the temperature dependence of the width is shown. This also shows that the inverse of the width i.e. the size of the ordered-region becomes large as temperature approaches T_c. From the log-log plot of T_c-T versus the inverse of the width shown in Fig. 5(b), it is found that the slope is around -1/5; a tendency to diverge is seen but it is rather weak. Theoretically, Langer discussed critical behavior of the time constant and that of the size of the ordered-region; he obtained the value of -1 as the former exponent.[8] Furthermore, Suzuki also proposed $(T_c-T)^{-1}$ dependence of the time constant in his scaling theory of the growth of order.[9] However, the correspondence of these theories with experiment is not clear for the time being. More extensive work is necessary.

Although the analysis of this experiment is still preliminary, the results show a lot of new interesting aspects of the kinetics of order-disorder phase transition. In the near future, detailed analysis will be done.

References

1) M. R. Collins and H.C. Teh: Phys. Rev. Lett. 30 (1973) 781.
2) N. Wakabayashi: unpublished.
3) S. M. Allen: Acta. Metall. 27 (1979) 1085.
4) K. Kawasaki, M. C. Yalabik and J. D. Gunton: Phys. Rev. A17 (1978) 455.
5) T. Hashimoto, K. Nishimura and Y. Takeuchi: J. Phys. Soc. Jpn. 45 (1978) 1127.
6) Y. Noda, S. Nishihara and Y. Yamada: J. Phys. Soc. Jpn. 53. (1984) 4241.
7) H. Furukawa: Phys. Lett. 97A (1983) 346.
8) J. S. Langer: Ann. Phys. 41 (1967) 108.
9) M. Suzuki: Adv. Chem. Phys. 46 (1981) 195.

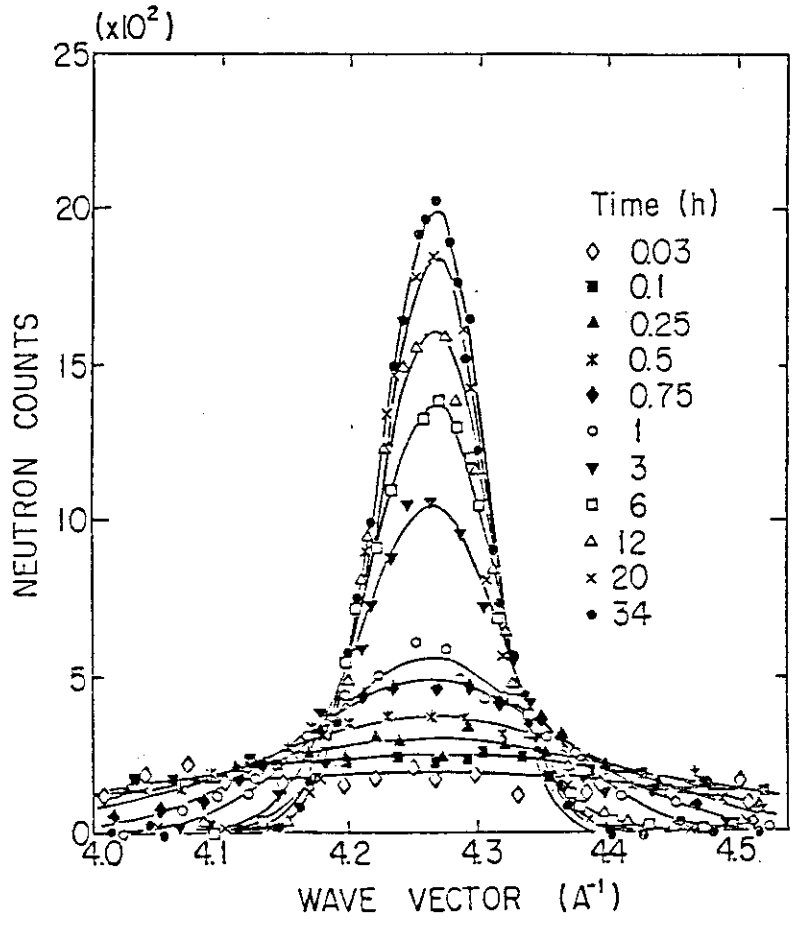

Fig. 1. Time dependence of the (211) superlattice peak of Ni_3Mn.

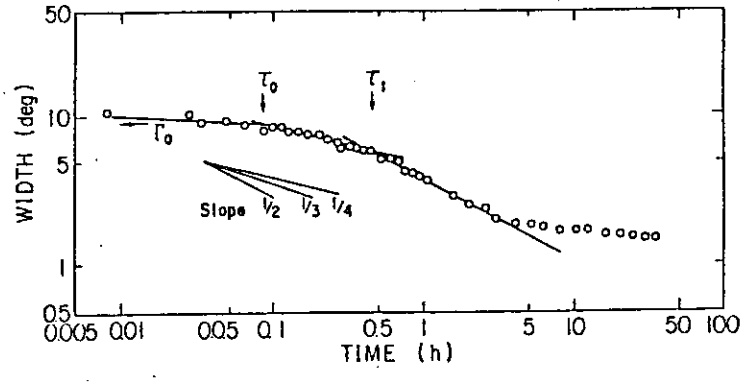

Fig. 2. Time versus width. The exponent of the power-law shows cross-overs at τ_0 and τ_1. (Γ_0 indicates the the width at τ_0.)

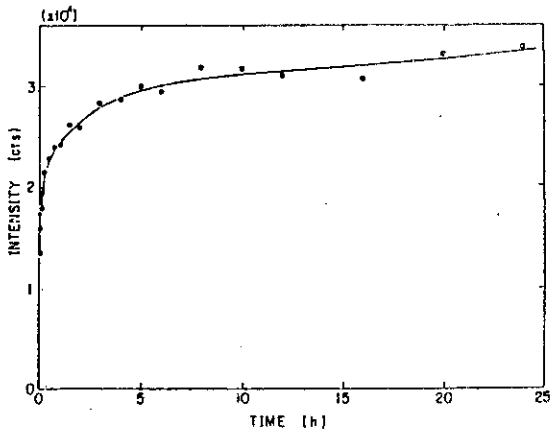

Fig. 3. Time versus Integrated intensity.

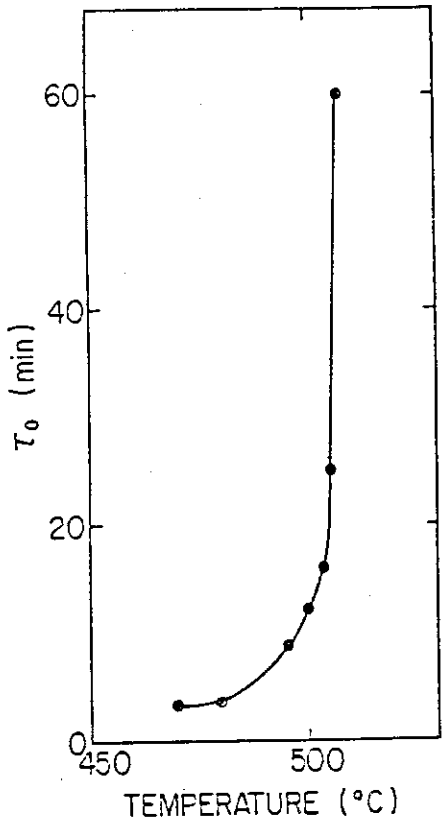

Fig. 4(a). Temperature versus the time τ_0 from when the width begins to follow the power-law of the exponent of 1/4.

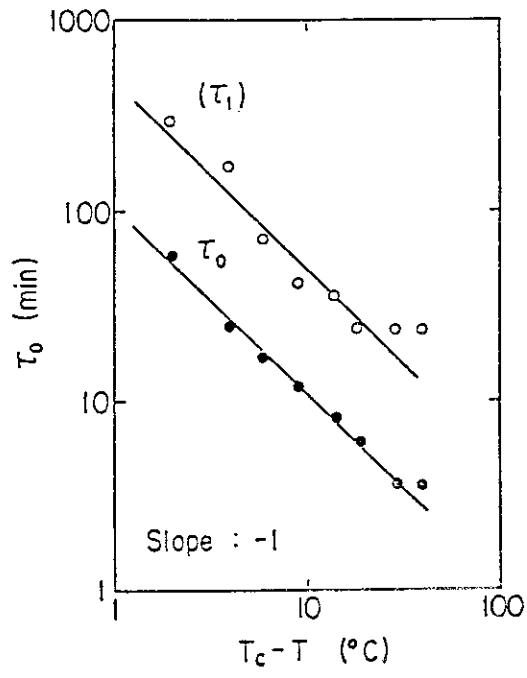

Fig. 4(b). Log-log plot of T_c-T versus τ_0. For reference, the time τ_1 from when the width begins to show the power-law of the exponent of 1/2 is also shown.

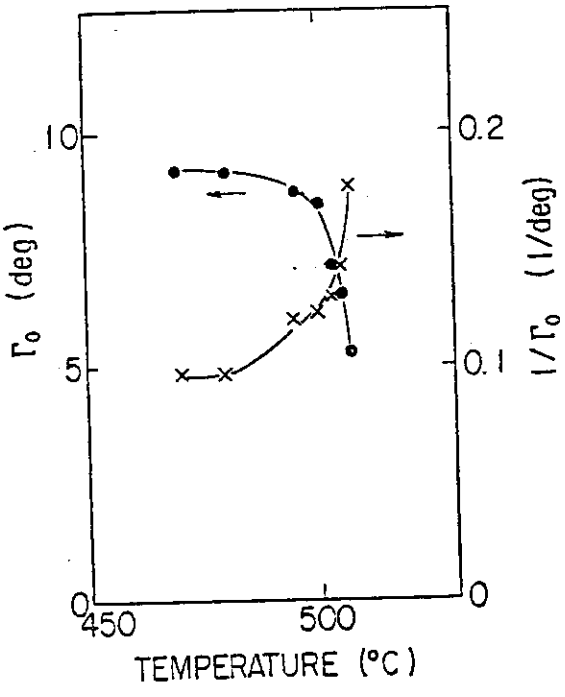

Fig. 5(a). Temperature versus the width at the time τ_0 and the inverse of it.

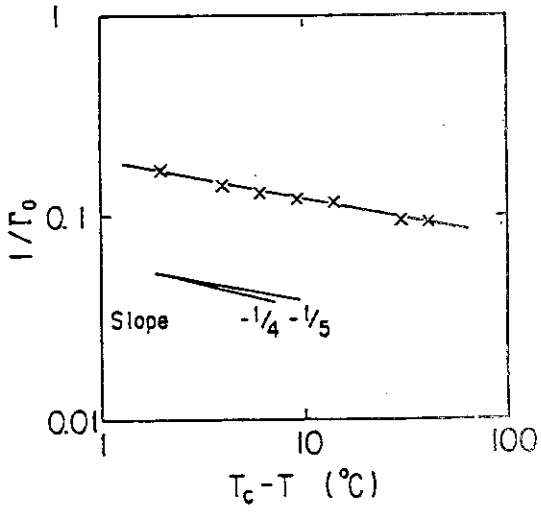

Fig. 5(b). Log-log plot of T_c-T versus the inverse of the width.

4. USE OF WIDE-ANGLE NEUTRON DIFFRACTOMETER FOR SINGLE-CRYSTAL DIFFRACTION IN FLAT-CONE METHOD

M. Iizumi, S. Funahashi, S. Katano,
Y. Morii, H. R. Child and R. M. Nicklow

One of the unique features of the wide-angle diffractometer is readily visible when the machine part of the diffractometer is tilted as a whole as is shown in the photograph on the front page of this progress report and also in Fig. 1 of this section. The strange arrangement is adopted in order to realize the inclination geometry in the single-crystal diffraction. By this geometry one can take full advantage of the curved one-dimensional position-sensitive counter to collect Bragg reflections or diffuse scattering data on a specific "layer" of the reciprocal space in a very efficient manner. In this mode of utilization the wide-angle neutron diffractometer can be regarded as a kind of diffraction camera which is comparable to the X-ray Weissenberg camera.

The "photograph" of the scattered neutron distribution on a zone (zero layer) is obtained as Fig.2(a) indicates; namely first mount the sample crystal with the zone axis perpendicular to the scattering plane on which both the incident beam and the curved linear counter lies; and then rotate the crystal around the zone axis continuously or step-wisely; then the "photograph" is obtained not by the development of films but by the computer data-processing of a series of diffraction patterns measured for successive angles of rotation.

Then what if the scattering not on the zero level of the reciprocal space is to be measured by efficient use of the curved linear counter ? It is then important to take it into account that the reciprocal space consists of a series of "layer" and to arrange the counter and the crystal axis in such a way that every point on the central level of the curved counter "sees" the same layer of the reciprocal space in the course of continuous or step-wise rotation of the crystal axis.

Here a few words about the "layer" will be in order. A layer or a level, means a plane in the reciprocal space which is perpendicular to the crystal rotation axis. This axis is usually chosen to coincide with one of the zone axes of the crystal. Then the reciprocal lattice consists of

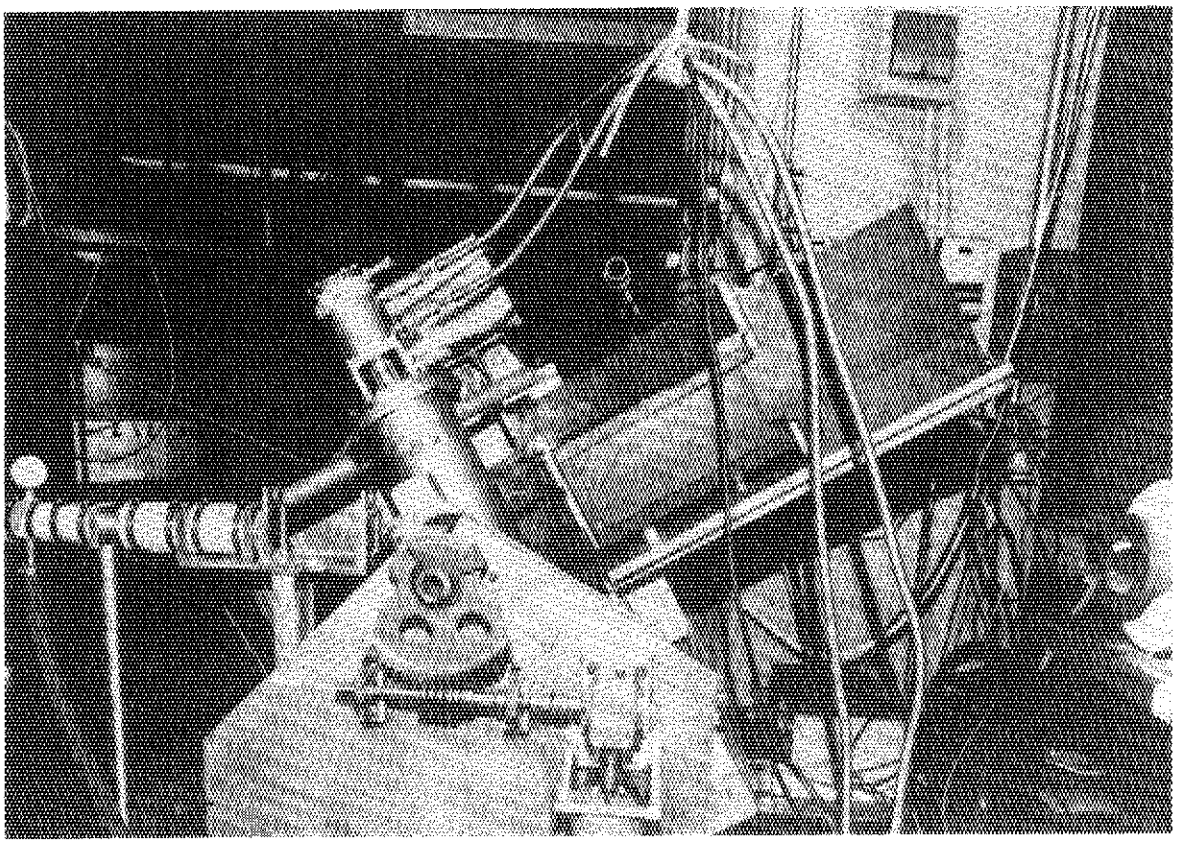

Fig. 1. Counter and crystal table assembly of wide-angle neutron diffractometer in the inclination arrangement. The shaft and the gear system for driving the inclination angle is seen in the front.

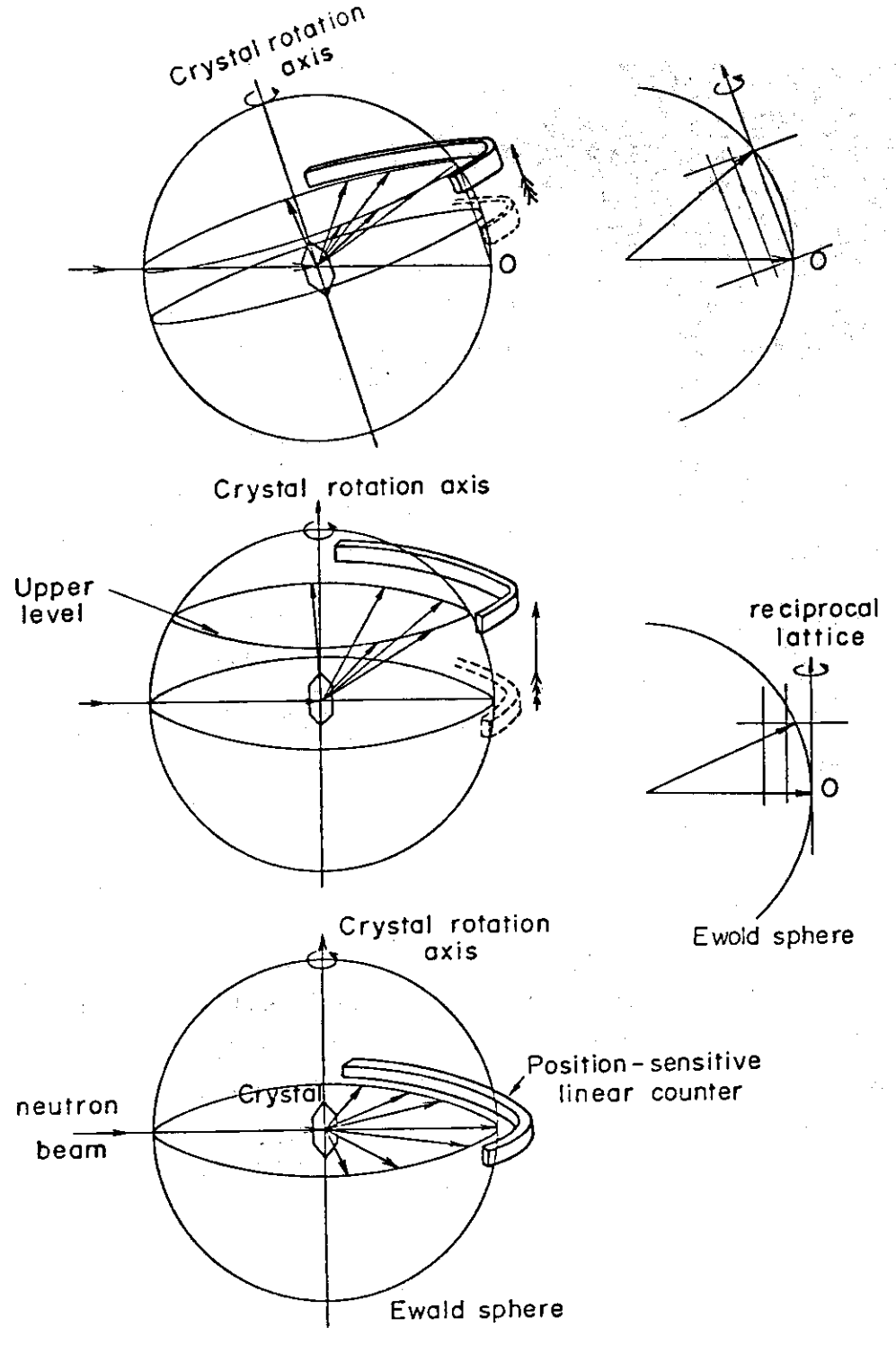

Fig. 2. Use of the curved one-dimensional counter in (a) the equatorial geometry (bottom), (b) the normal beam geometry (middle) and (c) the inclination geometry (top).

stacking of two dimensional lattices all of which perpendicular to the rotation axis. They are numbered one, two,... layer, or level, in order of the separation upward from the zero level. The layers below the zero level are minus one, minus two,... level. For example if we take the [001] axis of an orthorhombic crystal as the rotation axis then all the (h,k,ℓ) points with fixed ℓ constitute the ℓ layer, or ℓ level.

One of the arrangement of the counter to see the upper level simultaneously is to lift the counter from the zero level (or the equatorial plane of the Ewald sphere) as is shown in Fig. 2(b). An alternative method is to tilt both the crystal and the counter by the same angle. The combination of the lift-up and the tilt leads to the general inclination geometry of single-crystal diffraction (Fig. 2(c) and Fig. 3). The inclination gives rise to the angle designated as μ and the lift-up to the angle ν. Special choice of the combination of μ and ν are endowed with names which are shown in Fig. 3.

The equi-inclination arrangement is favorable in principle since there is no blind area. However, the flat-cone arrangement is more favorable from the practical point of view, since scattered neutrons impinge perpendicularly on the counter, which secures a proper response of the counter as well as a tight collimation and shielding of the counter. In the flat-cone arrangement the incident beam makes a certain angle with respect to the counter plane in such a way that the scattered neutrons from the level to be measured are always normal to the crystal axis and make a "flat cone".

In the wide-angle neutron diffractometer the base plate which holds the crystal table and the counter is tilted as a whole by a motor drive around the horizontal axis crossing the neutron beam perpendicularly at the sample position. There is an arbitrariness about the choice of the tilt axis, which is not necessarily perpendicular to the neutron beam. But this choice of the axis is most convenient since μ coincides with the tilt angle.

Practical methods of planning the diffraction geometry and of the data process are described by S. Funahashi in a separate report. Here the experiences gained by some examples are given.

Alignment of a single crystal by using the wide-angle counter was quite a new experience. The zone axis was aligned by adjusting the tilt

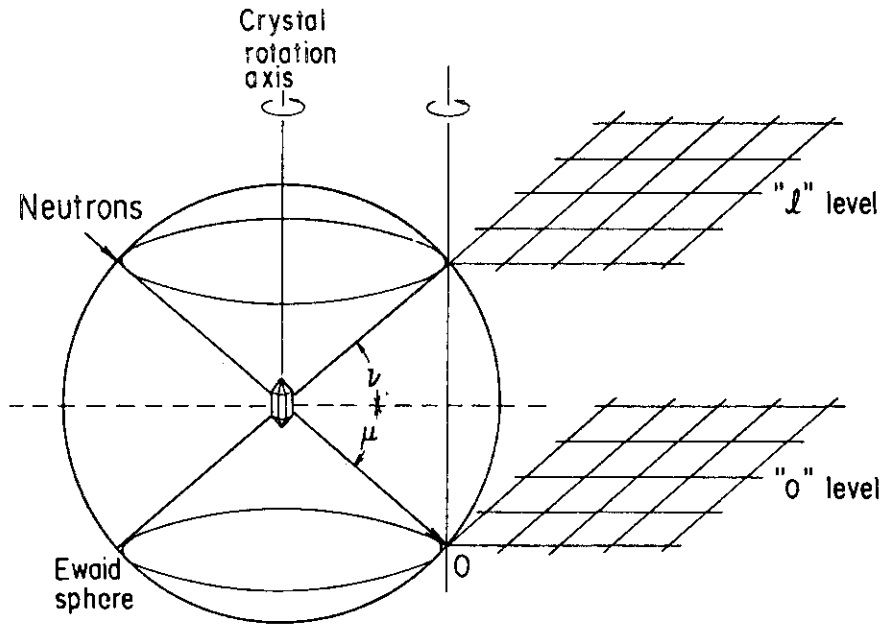

Inclination Geometry

$\mu = \nu = 0$	Normal beam , equatorial
$\mu = 0 , \nu \neq 0$	Normal beam
$\mu \neq 0 , \nu = 0$	Flat - cone
$\mu = \nu \neq 0$	Equi - inclination

Fig. 3. Definition of angles μ and ν and various kind of inclination geometry. In the wide-angle neutron diffractometer the flat-cone geometry is adopted where $\nu = 0$.

angles of the crystal goniometer after finding specific reflections at the proper scattering angles (2θ) along the circle of the counter. In this process the total intensity of the counts displayed by a rate meter was used. Contrary to the anticipation this was quite sensitive means of adjusting the specific Bragg reflections as is the case in the usual single-counter diffractometer. Proper adjustment of ω readings with the reciprocal axes could have been done but we simply started measurements based on the approximate estimate of the orientation of the crystal around the zone axis and the reciprocal lattice was assigned after getting an intensity map of the measured plane.

Two series of measurements have been carried out; one on a copper alloy to observe satellite spots related to the martensite embryo, the other on a ferroelectric crystal having an incommensurate phase to demonstrate the capability of observing the diffraction on the upper levels of the reciprocal lattice.

The zero level diffraction from the $Cu_{68}Al_{28}Ni_4$ alloy single crystal was observed with the choice of the [001] axis as the crystal rotation axis. The results are indicated in the Funahashi's report on the data processing (Fig. 4). One of the figures is reproduced here in Fig. 4. At the temperature a little bit lower than room temperature this crystal gives rise to a martensitic phase transition which is related to the shape-memory effect in this alloy. The nature of lattice instability of the alloy was studied by the present authors[1] and then pointed out that some sign of pretransitional phenomena is seen in the elastic satellite reflections in the parent cubic phase. The purpose of the present observation by the wide-angle neutron diffractometer was to extend the observed region of the reciprocal space from lines to planes. The results indicates that the satellite reflections are observed at only a limited number of points. The satellite spot at (2+1/3,2-1/3,0) seen in the Fig. 4 is one of the example of them. Detailed observation of the scattering is now in progress.

We must admit that we are in a very elementary stage of the instrument utilization for this kind of measurements and there are a lot to be done in future to improve the quality of the observation. But it is surprising that even in this stage we did observe something beyond our expectation. This is the thermal diffuse streak along the [1,-1,0] lines

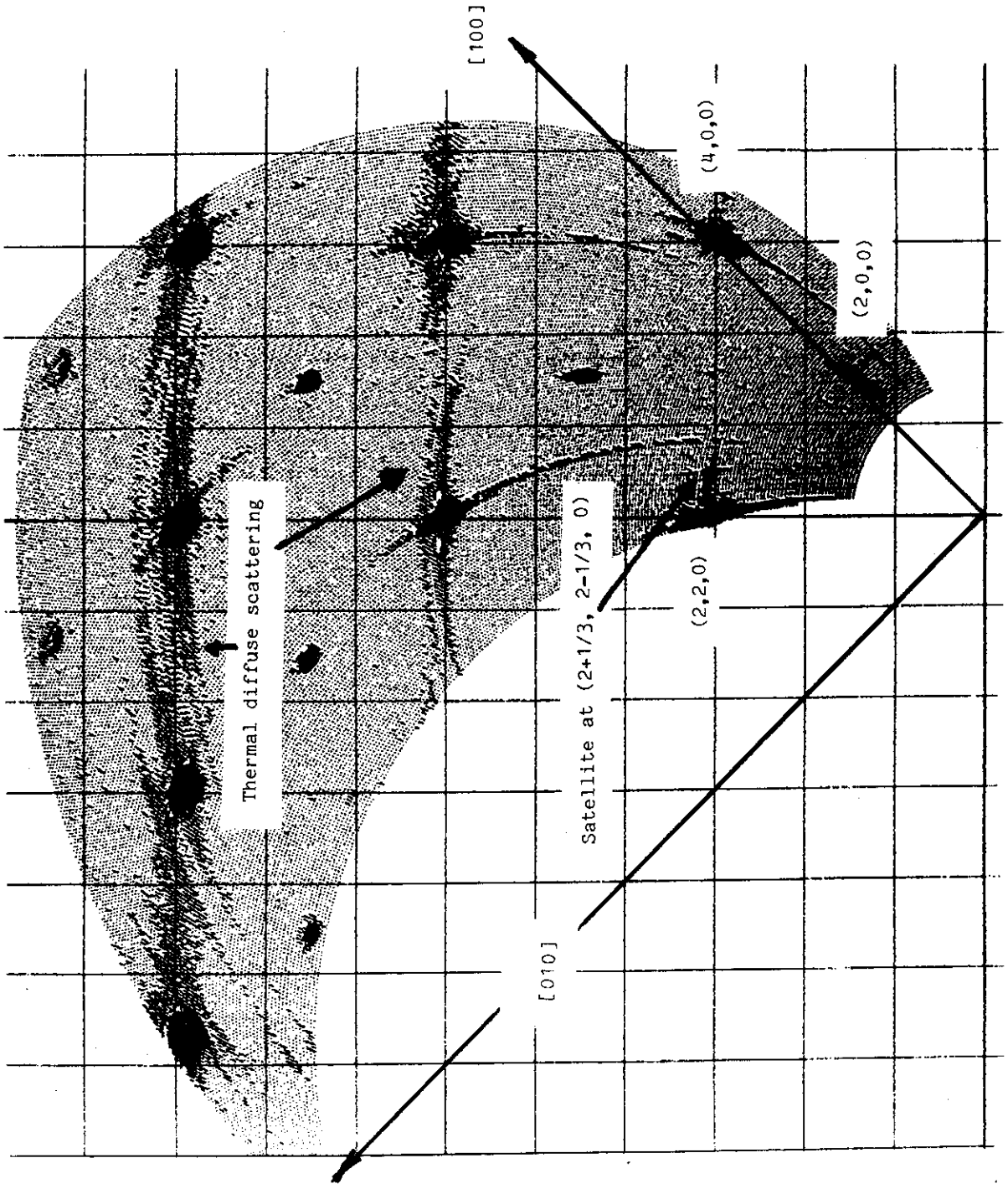

Fig. 4. Single crystal diffraction map of the zero level of $Cu_{68}Al_{28}Ni_4$ crystal for the [001] rotation axis. The satellite scattering due to the martensite embryo is seen on the $[1\bar{1}0]$ lines and the thermal diffuse scattering forms streaks extending along the $[1\bar{1}0]$ axes.

connecting the fundamental reflections.

This crystal has extraordinary low transverse phonon energies along the [110] direction and this is closely related to the lattice instability which gives rise to the martensitic phase transition. The dispersion surface including the low-lying phonons forms a deep valley in the vicinity of the [110] axis. This feature of the phonon dispersion surface[1] explains the streak-like diffuse scattering observed in the present work. This is the first neutron diffraction observation of the diffuse scattering map of this sort.

The second example of the single-crystal measurement is on the incommensurate reflections in Rb_2ZnBr_4. This crystal has an incommensurate phase between 190 to 350 K. The incommensurate reflection appears at $(h,k,l + (1/3 - \delta))$ with $\delta = 0.04$[2]. In this case the observation of the upper level reflections were tried by mounting the single crystal specimen with the [010] axis vertical and then the diffractometer was tilted by an angle (15°) which brought the second level, $(h,2,l)$ reciprocal plane to the flat cone geometry. The result was indicated in Fig.5 of the Funahashi's report. The weak satellite reflections are clearly visible at the incommensurate positions. This results have demonstrated the invaluable potentiality of the wide-angle diffractometer in searching such a kind of reflections whose positions are unknown.

1) Y. Morii and M. Iizumi, J. Phys. Soc. Jpn. 54, 2948 (1985).
2) K. Gesi and M. Iizumi, J. Phys. Soc. Jpn. 45, 1777 (1978).
also see M. Iizumi and K. Gesi, J. Phys. Soc. Jpn. 52, 2526 (1983).